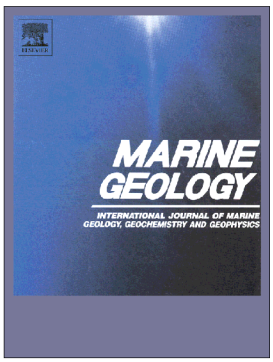

Submarine morpho-structure and active processes along the North American-Caribbean boundary plate (Dominican Republic sector)

A. Rodríguez-Zurrunero, J.L. Granja-Bruña, A. Carbó-Gorosabel, A. Muñoz-Martín, J.M. Gorosabel-Araus, L. Gómez de la Peña, M. Gómez Ballesteros, A. Pazos, M. Catalán, S. Espinosa, M. Druet, P. Llanes, U. ten Brink

PII: S0025-3227(18)30295-0
DOI: https://doi.org/10.1016/j.margeo.2018.10.010
Reference: MARGO 5866

To appear in: *Marine Geology*

Received date: 13 July 2018
Revised date: 17 October 2018
Accepted date: 25 October 2018

Please cite this article as: A. Rodríguez-Zurrunero, J.L. Granja-Bruña, A. Carbó-Gorosabel, A. Muñoz-Martín, J.M. Gorosabel-Araus, L. Gómez de la Peña, M. Gómez Ballesteros, A. Pazos, M. Catalán, S. Espinosa, M. Druet, P. Llanes, U. ten Brink , Submarine morpho-structure and active processes along the North American-Caribbean boundary plate (Dominican Republic sector). Margo (2018), https://doi.org/10.1016/j.margeo.2018.10.010

To be submitted to Marine Geology

Submarine morpho-structure and active processes along the North American-Caribbean boundary plate (Dominican Republic sector)

A. Rodríguez-Zurrunero, (1*), J.L. Granja-Bruña, (1), A. Carbó-Gorosabel (1), A. Muñoz-Martín (1,2), J.M. Gorosabel-Araus (1), L. Gómez de la Peña (3), M. Gómez Ballesteros (4), A. Pazos (5), M. Catalán (5), S. Espinosa (6), M. Druet (7), P. Llanes (1), U. ten Brink (8).

*Corresponding author: arzurrunero@ucm.es

(1) Applied Tectonophysics Group. Department of Geodynamics, Stratigraphy and Paleontology. Universidad Complutense, Madrid, Spain

(2) Instituto de Geociencias (UCM, CSIC), Madrid, Spain

(3) GEOMAR Helmholtz Centre of Ocean Research, Kiel, Germany.

(4) Instituto Español de Oceanografía, Madrid, Spain

(5) Real Instituto y Observatorio de la Armada, San Fernando, Cádiz, Spain

(6) Instituto Hidrográfico de la Marina, Cádiz, Spain

(7) Instituto Geológico y Minero de España, Tres Cantos, Madrid. Spain.

(8) U. S. Geological Survey Woods Hole. MA. USA.

Abstract

The northern margin of Hispaniola records the oblique collision/underthrusting of the Bahamas Carbonate Province with the island-arc. Due to the collision, northern Hispaniola has suffered several natural disasters caused by major earthquakes and tsunamis, such as the historic earthquake of 1842, the tsunami caused by earthquake-driven slumping in 1918 in the Mona Passage, the seismic crisis of 1943-1953 with five events of M>7.0 or the seismic crisis of 2003 with a main shock of M6.3 and a large aftershock of M5.3. Using new swath multibeam bathymetry data and vintage single- and multi-channel seismic profiles, we have performed a regional scale analysis and interpretation of the shallow surface and active processes along the northern margin of the Dominican Republic. We have identified three morphostructural provinces: a) the Bahamas Banks, b) the Hispaniola Trench and c) the Insular Margin, which are divided into two tectonic domains, the Collision Domain and Underthrusting Domain. The southern slope of the Bahamas Carbonate Province shows a very irregular morphology produced by active erosive processes and normal dip-slip faulting, evidence of an extensional tectonic regime and margin collapse. This collapse is of major extent in the Oblique Collision Domain where there are erosive and fault escarpments with higher dip-slip fault throws. The Hispaniola Trench, is formed by the Caicos and Hispaniola basins in the underthrusting domain, and by the Santisima Trinidad and Navidad basins in the Oblique Collision Domain. They have a flat seafloor with a sedimentary filling of variable thickness consisting of horizontal or sub-horizontal turbiditic levels. The turbiditic fill mostly proceeds from the island arc through wide channels and canyons, which transports sediment from the shelf and upper slope. The Insular Margin comprises the Insular Shelf and the Insular Slope. The active processes are generated on the Insular Slope where the Northern Hispaniola Deformed Belt is developed. This Deformed Belt shows a very irregular morphology, with a WNW-ESE trending N verging imbricate thrust-and fold system. This system is the result of the adjustment of the oblique collision/underthrusting between the North American plate and the Caribbean plate. In the Oblique Underthrusting

Domain the along-strike development of the imbricate system is highly variable forming salients and recesses. This variability is due to along-strike changes in the sediment thickness of the Hispaniola Trench, as well as to the variable topography of the underthrusting Bahamas Carbonate Province. In the Oblique Collision Domain, the morphology of the Insular Slope and the development of the Deformed Belt deeply change. The imbricate system is barely inferred and lies upslope. These changes are due to the active collision of Bahamas Carbonate Province with the Insular Margin where the spurs are indented against the Insular Margin. Throughout the entire area studied, gravitational instabilities have been observed, especially on the Insular Margin and to a lesser extent on the southern slope of the Bahamas Carbonate Province. These instabilities are a direct consequence of the active underthrusting/collision process. We have mapped large individual slumps north of Puerto Plata in the Oblique Underthrusting Domain and zones of major slumps in the Oblique Collision Domain. These evidences of active processes must be considered as near-field sources in future studies on the assessment of tsunami hazards in the region.

Keywords: Caribbean Plate, Hispaniola, shallow structure, active processes, collision, earthquake, tsunami.

1. Introduction

The significant increase in population density in coastal areas and the growing development of offshore infrastructures make the study of active geological processes in the nearby seafloor essential to assess the associated geological hazards (e.g., earthquakes, gravity instabilities and tsunamis; Chiocci et al., 2011; Hough et al., 2011). This is the case of the northern coast of Dominican Republic, which shows a great tourist development with large population centers, as the city of Puerto Plata with ≈ 330,000 inhabitants. The limited preparation of the majority of citizens and the lack of risk reduction strategies, put the population and economy of coastal areas of Hispaniola at substantial risk in case of large earthquakes and tsunamis (IOC Workshop Reports No. 255, 2013; and No 276, 2016; von Hillebrandt-Andrade, 2013). The northern Hispaniola region has suffered several disasters as the historic large earthquake of 1842 (McCann, 2006) and the seismic crises of 1943-1953 and 2003 (Russo and Villaseñor, 1995; Dolan et al., 1998; Dolan and Bowman, 2004). In addition, after the event of August 4th, 1946 a tsunami struck the Bahía Escocesa causing significant damages (O'Loughlin and Lander, 2003 and references therein). Tsunami simulations carried out in the northern coast of Hispaniola have provided important level of tsunami hazard in case of large tsunamigenic events nucleated in the North American-Caribbean (NOAM-CARIB) boundary plate. However, simulations considered several scenarios based on not clearly established seismogenic sources and an incomplete historical tsunami records (Gailler et al., 2015; Grilli et al., 2016). Damage location and significance of events recorded in historical chronicles contain useful information on the event location, but are likely biased by the local subsurface geology and the location of the main population centers at the time of the event (Gailler et al., 2015). On the other hand, tsunami simulations have not considered near-field tsunami sources related with slumping driven by earthquakes and/or steep seafloor slopes that have been recently documented as major contributors to tsunami hazard (Synolakis et al., 2002; Okal et al., 2009). Tsunamis caused by

earthquake-driven slumping also occurred around Hispaniola, such as the 1918 one in the Mona Passage (López-Venegas et al., 2008)

The northern Dominican Republic offshore margin was explored in the 80s and 90s of the 20th century from GLORIA large-range side-scan sonar, low-resolution single-channel seismic data (Dolan et al., 1998), and some sparse multi-channel seismic profiles from industry, obliquely oriented to the tectonic structure of the margin (Dillon et al., 1992, 1996). That information has provided a limited knowledge of the morphology and the structure of the margin. The compressional nature and the major features of the margin like the North Hispaniola Deformed Belt (NHDB) are known, but low resolution of data make difficult a good characterization of active processes along and across the margin. Because of that, at the end of 2013 a marine geophysical cruise was carried out aboard the Spanish R/V Sarmiento de Gamboa. This cruise combined the systematic acquisition of geophysical data throughout the oblique convergent NOAM-CARIB boundary plate, mainly offshore of Dominican Republic, providing continuous and high-resolution data, which complete coverage of this segment of the Caribbean-North America plate boundary, and reveal with unprecedented detail the features of the morphology and shallow structure.

The main goal of this study is to carry out a regional-scale analysis and interpretation of the shallow structure and active processes along the Dominican sector of NOAM-CARIB boundary plate (Fig. 1). This goal has been addressed by a combined interpretation of new high-resolution multibeam bathymetry data, GEBCO and SRTM databases, and reprocessed vintage 2D single- and multi-channel seismic reflection data. This study provides a detailed identification and interpretation of the active tectonic and sedimentary processes along and across the plate boundary. This information allows the detailed characterization of potential near-field tsunamigenic sources (i.e., seafloor faulting and submarine slumping) that are the basis for future realistic studies on the assessment of tsunami hazard in the region, as well as for practical

implementation of tsunami preparedness and protection, and for coastal planning and marine resources use in the Dominican Republic. Northern coasts of Haiti and Dominican Republic are in obvious risk because of the proximity of the potential tsunamigenic sources to the coastal areas (30– 50 km), resulting in a very short lead-time for response (IOC Workshop Report No. 255, 2013).

2. Tectonic Setting

The Hispaniola Island belongs to the Greater Antilles island arc together with Puerto Rico, Jamaica and Cuba. This island arc together with the Lesser Antilles island arc, works as a geographic limit between the Caribbean Sea and the Atlantic Ocean. Along the northern margins of Hispaniola and Puerto Rico, oblique convergence between the NOAM and CARIB plates is taking place with CARIB plate moving eastward (70º) at a rate of 18-20 ± 3 mm/yr. (Fig. 1; DeMets et al., 2000; Mann et al., 2002; Calais et al., 2016). Oblique convergence is accommodated by subduction along the E-W oriented Puerto Rico Trench (8,300 m-deep), and by collision-underthrusting along the WNW-ESE oriented Hispaniola Trench (4,000 m-deep). The east-to-west transition from the Puerto Rico to the Hispaniola trenches has yielded a segmented margin plate where the transition from oblique subduction to collision-underthrusting takes place (Calais et al., 2016). The main geomorphic features of this change are the northward shift of the NOAM-CARIB plate boundary, the significant decrease in depth of the trenches and the change in orientation from E-W to ENE-WSW. This change is located where buoyant continental crust of the Bahamas Carbonate Province (BCP) reaches the convergent plate boundary because of the relative displacement between the NOAM and CARIB plates (Fig.1). The study region only embraces the southeastern termination of the large BCP (Fig. 1; Mullins et al., 1992), that consists of coalesced carbonate banks separated by wide and deep passages (Eberli and Ginsburg, 1987). As a result of plate convergence, the relative thicker crust of the BCP behaves

as a tectonic asperity slowing down and blocking the true subduction observed eastward in the Puerto Rico Trench. The result is a 350 km-long segment along the Northern Hispaniola Margin where the oblique collision and underthrusting between the NOAM and CARIB plates takes place (Dolan et al., 1998; Mann et al., 2002; Calais et al., 2002; Pérez-Estaún et al., 2007; Calais et al., 2016; Fig. 1). The collision process, since its beginning in the Eocene, has conditioned every structural, seismological, and sedimentological feature in the northern margin of the CARIB plate (Pindell and Barrett, 1990; Dolan et al., 1998; Mann et al., 2002).

Because of convergence, south of the Hispaniola Trench is located the compressive Northern Hispaniola Deformed Belt (NHDB), which constitutes a N-verging fold-and-thrust system sub-parallel to the trench (Fig. 1; Dillon et al., 1996; Dolan et al., 1998). Block modeling of GPS velocities indicates that NHDB is building up elastic strain at a rate of 1-3 mm/yr. (Fig. 1; Calais et al., 2002; Manaker et al., 2008; Calais et al., 2010; Benford et al., 2012). Onshore, oblique convergence is fundamentally accommodated by the Septentrional-Oriente Fault Zone (SOFZ; Calais et al., 2002). The Hispaniola segment of the SOFZ is the Septentrional Fault Zone (SFZ) that is characterized by paleo-seismological studies and block modeling of GPS velocities as an active left-lateral strike-slip fault that accommodates 10-12 mm/yr. of deformation along E-W direction (Fig. 1; Prentice et al., 2003; Manaker et al., 2008; Calais et al., 2010). Therefore, the coexistence of the NHDB that accommodates the shortening component, and the SFZ that accommodates along-strike component can be understood in a strain partitioning model (Mann et al., 1995, 2002; Calais et al., 2002; ten Brink and Lin, 2004;).

The active oblique collision/underthrusting process has been associated with the frequent occurrence of earthquakes along the Northern Hispaniola Margin, highlighting the May 7th, 1842 event with M8.0 (McCann, 2006; M7.8 by Russo and Villaseñor, 1995: M7.6 by ten Brink et al. 2011), the seismic crisis of 1943-1953 with five events of M>7.0 and the seismic crisis of 2003 with a main shock of M6.3 and a large aftershock of M5.3 (Dolan and Bowman, 2004). The May

7th, 1842 event was a tsunamigenic earthquake that struck the northwestern Hispaniola region causing 5000 fatalities in Cap-Haitien (Scherer, 1912). The tsunami caused ~300 deaths with wave heights of ~2m along the northeastern Haitian coast and a maximum run-up of 4.6 m in Port-de-Paix (O'Loughlinnd and Lander, 2003). This event is commonly associated with the strike-slip on the SFZ, but recent tsunami simulations strongly suggests that the source could be mostly related with a rupture along the NHDB (Gaillier et al., 2015). The event of August 4th, 1946 occurred in northeast Hispaniola, with M8 (M8.1, Dolan et al., 1998; M7.8, Russo and Villaseñor, 1995), was probably the largest event to strike the area since at least 1564 (Chalas-Jimenez, 1989). It was followed by a tsunami that mainly hit the coast of the Bahía Escocesa (Lynch and Bodle, 1948). The M6.4 earthquake on September 22th, 2003, did not cause a tsunami, but triggered a seismic crisis that shook the northern part of the Hispaniola near Puerto Plata (300,000 inhabitants) causing substantial material damage that extended up to 30 km to the South, in the city of Santiago de los Caballeros (over 500,000 inhabitants; Dolan and Bowman, 2004). Model slip rates based on GPS-derived velocities (Manaker et al., 2008; Ali et al., 2008), suggest that both SFZ and NHDB are currently accommodating elastic strain, being the potential sources of significant earthquakes that could affect the coastal areas of Hispaniola, through ground shaking and/or tsunami inundation (Gailler et al., 2015)

3. Materials and methods

The methodology was based on a combined analysis and interpretation of new high-resolution multibeam bathymetry data, reprocessed vintage 2D single- and multi-channel seismic reflection data, and published GLORIA side-scan sonar images (Dillon et al., 1992; Dolan et al., 1998). The northern regions of the study area not covered by high-resolution swath bathymetry data have been interpreted based on the seismic profiles and the geo-referenced images of GLORIA large-range side-scan sonar (Dillon et al., 1992; Dolan et al., 1998). Most of the study region was

systematically mapped during the NORCARIBE geophysical cruise in November-December 2013 aboard the Spanish R/V Sarmiento de Gamboa using the hull-mounted multibeam Hydrosweep ATLAS DS echo-sounder system. The survey covered an area of approximately 15,000 km^2, between water depths of -500 and -4,300 m (Fig. 2 and App. A). The processed data was interpolated yielding a regular grid of 30 m-interval. The eastern region was completed with a 50 m-gridded multibeam data from a compilation of several USGS/NOAA cruises (Andrews et al., 2014). The multibeam bathymetry coverage has been completed with the GEBCO Digital Atlas with a 30 arc-second of resolution (Weatherall et al., 2015), and onshore data has been obtained from the SRTM mission with a 90 m of resolution (Far et al., 2007).

The 2D single- and multi-channel seismic reflection data, from the MW8908 (1989) and FM0503 (1980) cruises, were provided by two public databases (Fig. 3): The National Oceanographic and Atmospheric Administration National Centers for Environmental Information (www.ngdc.noaa.gov) and the Academic Seismic Portal managed by University of Texas-Institute for Geophysics (Christeson et al., 2017), respectively. The single-channel profiles from the MW8908 cruise were acquired with either one or two 120 c.i. air guns and the processing of the seismic reflection data included deconvolution, automatic gain control, low-cut frequency filters, and a ramp filter designed to remove ship noise (Dolan et al., 1998). The single-channel seismic data from the MW8908 cruise are scanned microfilm images obtained from the original paper records. To be used in the present study we carried out a detailed image editing with enhancement by digital filters. The multi-channel seismic profiles of the FM0503 cruise were acquired with the NAVITAT satellite navigation system (NAVSAT), shot interval each 35 m using 4 Bolt 4200 air-gun array with a total volume of 6000 c.i. The recording system consisted of a 3360 m-long digital streamer, with 48 channels regularly spaced to 70 m. The processing sequence from original data include Normal Move-out correction, Common Mid-Point gathering and stacking. In order to improve the signal-to-noise ratio, remove diffractions and restore

geometries, we have carried out a post-stack processing, including a post-stack Kirchhoff migration, F-X Deconvolution, Dynamic Signal-Noise Ratio and a seafloor muting.

4. Results

Based on similar morphological, structural and sedimentological criteria derived from the combined interpretation of high-resolution swath bathymetry and 2D reflection seismic data, and published GLORIA side-scan sonar images (Dillon et al., 1992; Dolan et al., 1998), the study area can be divided into three WNW-ESE trending morphostructural provinces: a) the Bahamas Carbonate Province (BCP), b) the Hispaniola Trench (HT) and c) the Insular Margin (IM) (Fig. 3, App. B). In addition, these provinces are divided along-strike into two tectonic domains (Fig. 3): The Oblique Collision Domain (OCD), which is defined as the region where buoyant carbonate spurs of the BCP are indenting into the island arc at the seafloor surface; and the Oblique Underthrusting Domain (OUD), in which high-standing carbonate reliefs of the BCP are buried beneath the sediments of the HT and the IM. The along-strike boundary between these two tectonic domains is marked where the Silver Spur impinges into the IM at the longitude of Rio San Juan Peninsula (Fig. 3). The significant effects of the indentation of the Silver Spur is recorded on-land with the remarkable uplift of the Cabrera Promontory (Fig. 5, App. A), consisting of 11 levels of southward-tilted marine terraces, faulted parallel to the deformation front (Diaz de Neira et al., 2017). These terraces show a continuous uplift at least from the Lower Pleistocene with uplift rates ranging 0.15-0.17 mm/yr. (Diaz de Neira et al., 2017).

The morphostructural interpretation to regional scale of the Underthrusting and Collision domains are shown in Figures 4 and 5, respectively.

4.1 Bahamas Carbonate Province (BCP)

The survey area covers the southeastern end of the BCP (See inset in Fig.1; Sykes et al., 1982; Eberli and Ginsburg, 1987; Mullins et al., 1992). While the northwestern BCP consists of large platform, and coalesced carbonate banks (Eberli and Ginsburg, 1987), the southeastern termination is characterized by isolated and irregular flat-topped reliefs, which rise from the surrounding abyssal plains located between 4,300 and 3,800 m of water depth (App. A). These reliefs are separated by wide channels, called "passages" in the bibliography, which connect the seafloor of the HT with the abyssal plains of the NOAM plate north of the BCP. In our study area, there are four large banks (from W to E); Mouchoir, Silver, Santisima Trinidad and Navidad banks (Fig. 3). The Mouchoir, Silver and Navidad banks present a wide flat-topped morphology with water depths of a few tens of meters and locally emerging in the form of patches and reef barriers, whereas the Santisima Trinidad bank consists of a NNE-SSW oriented ridge with a narrow flat-topped area (Fig. 3, Apps. A and C). In this study we interpret in more detail the southern slopes of BCP since they are partially covered with high resolution multibeam data, and extend the interpretation northwards based on seismic data and the published GLORIA side-scan sonar images (Dillon et al., 1992; Dolan et al., 1998).

4.1.1 Mouchoir Bank

The Mouchoir Bank is located northwards of the flat-floored Hispaniola and Caicos basins in the OUD (Fig. 4). The surveyed area of the Mouchoir Bank consists of two salients (Western and Eastern spurs) separated by an irregular zone featured by bankward amphitheater-shaped morphologies ("scallops"; Mullins and Hine, 1989). Between the spurs, there is a marginal or isolated relief disconnected from the south slope of the bank (Fig. 4). Similar isolate reliefs have also been identified out of our survey area, in the northern flanks of the BCP, from GLORIA side-scan sonar data (Mullins et al., 1992; Dolan et al., 1998).

The morphology of the Western and Eastern spurs is characterized by a series of high-standing reliefs and terraces flanked by structural and erosive steep escarpments (15-35º-dip) (Fig. 4 and App. C). Structural escarpments are mainly W-E to WNW-ESE trending and are the result of recent normal fault activity with variable dip-slip throw (Figs. 6 and 7). Erosive escarpments are very sinuous but with a preferential E-W to NE-SW orientations. Interpreted GLORIA side-scan sonar images by Mullins et al. (1992) shows that these erosive escarpments are higher, longer and more frequent in the upper and middle slope of the banks (Fig. 4). These escarpments are distributed in 2-3 rows steeper downslope (App. C). Same as in spurs, some of these escarpments are controlled by normal faulting (Figs. 4, 6 and 8). Locally, GLORIA side-scan sonar data and seismic data allow to identify carbonate outcrops in some of these steep escarpments (Figs. 4, 7 and 8). They are found in the middle-lower slope of the Mouchoir Bank and in the lower parts of the Marginal Relief and Mouchoir Eastern Spur. The carbonate outcrops are shown in GLORIA data as high reflective zones and as transparent seismic facies in single- and multi-channel seismic lines. Mouchoir Western Spur is not covered with GLORIA data and seismic data do not show transparent seismic facies in the escarpments, but probably carbonate outcrops might locally occur (Fig. 4). Widespread erosive features, as small gravity failures, show more occurrence nearby erosive and fault escarpments. Small canyon/gully systems are mostly developed in the western and eastern flanks of the spurs. Only one well-developed canyon system was identified in the surveyed area, connecting the upper slope of the Mouchoir Bank with the HT seafloor (Fig. 4). These main channels are identified by GLORIA side-scan sonar data and are found preferably in the most developed scallops, where erosion has progressed further to the north. It is worth highlighting a huge area of debris flows flanked eastward by the cited large canyon system (Fig. 4; Dolan et al., 1998). GLORIA data reveal chaotic reflectivity, which passes downslope into well-developed lineation that are interpreted as flow-lines produced by a large (50 km-long, 25 km-wide) debris flow deposit (Mullins et al., 1992). Unfortunately, high-resolution swath bathymetry does not cover this region, and GEBCO data only allows to infer a

smooth convex morphology (Fig. 2). The large canyon that flanks the debris flow to the east, shows a truncate path probably caused for the canyon erosion. Between the Western and Eastern spurs, there is a marginal relief forming a seamount that raises more than 1,000 m from the Hispaniola Basin seafloor (Figs. 4 and 8). Since this feature is not fully covered by high-resolution swath data, and the resolution provided by the satellite-derived bathymetry is very limited, its shape cannot be defined in detail. However, seismic data show that the internal structure resembles the same extensional framework of normal faults previously described for the Western and Eastern Spurs (Fig. 8). It seems feasible that this marginal relief is the relict of a largely eroded ancient spur. These observations suggest that the morphology of the Mouchoir Bank slope is mainly controlled both active normal faulting parallel to the boundary plate and erosive processes.

The seismic sections allow to observe an internal structure that are preserved from deformation and erosion in the northward and shallower regions of the bank slope (Figs. 6 and 8; see enlargements). Here, the internal structure consists of two high-reflective seismic units (Figs. 6 and 8): an upper unit displaying continuous, parallel and high-amplitude reflectors defining a 0.3-0.5 sTWT-thick sediment package; and a lower seismic unit consisting in a 0.2-0.4 sTWT-thick package of discontinuous low-amplitude reflectors that progressively becomes transparent. The internal structure of the Western and Eastern spurs and the marginal relief are roughly the same but intensely affected by faulting and erosional processes. This fact yields that the upper units are almost absent as in the marginal relief. Locally, along the slope of the banks and near the marginal reliefs, it can be observed a shallower seismic unit consisting 0.1-0.2 sTWT-thick package of sedimentary reflectors interbedded by chaotic facies probably related with slope processes (i.e., channel fills, fans, slumping and drift deposits; Figs. 8 and 10).

4.1.2 Silver, Santísima Trinidad and Navidad banks

Silver, Santísima Trinidad and Navidad banks are located in the OCD. The Silver Spur impinges into the island arc, marking the eastern end of the Hispaniola Basin and the change between the Underthrusting and Collision domains (Fig. 5). The impingement of the Silver Spur takes place in a segment of 60 km-long, showing a terraced morphology like the observed in the Western spur of the Mouchoir Bank. These terraces are also a result of the dip-slip throw of numerous S-dipping normal faults (Figs. 5 and 9). The amount of the vertical fault throw is variable between tens to hundreds of meters, locally allowing carbonate outcrops. However, in the Silver Spur the orientation of the faults is more WSW-ENE trending than in the Mouchoir Bank.

Santisima Trinidad Bank is an elongate SSW-NNE trending bank (Figs. 2 and 5). Based on its morphology, this bank has suffered very high erosion that forms steep escarpments in all directions, allowing the outcrop of the carbonate basement. Between the reliefs, there are well-developed canyon systems that bypass the lower slope apron, reaching the Santisima Trinidad Basin through the Santisima Trinidad Passage. The lack of high resolution swath bathymetry data prevents to identify more accurately morphological and structural features along the bank.

The internal structure of the Silver and Santisima Trinidad spurs seems to be similar to that of the Mouchoir spurs, but in this case the lower resolution of the single-channel seismic data prevents a better characterization (Figs. 9, 10 and 15). In the lower slope of the spurs and in the bottom of the Navidad Passage, we have identified shallower seismic facies resulting from a complex interaction among slope, contour and bottom current processes (drift and slumping deposits; Fig. 9).

The Navidad Bank consists in a huge high-standing flat-topped carbonate relief, which has suffered very strong erosive dismantling along its southern edge (Fig. 5). This flank shows a steeped slope characterized by erosive and fault escarpments that locally allow the outcrop of the carbonate basement (Figs. 5, 11 and 12). Most fault scarps are E-W oriented, turning to ENE-

WSW in the eastern termination towards the Puerto Rico Trench by means of two large NE-SW normal faults. The extent of these erosive and fault escarpments is crossed by canyon systems that connects the carbonate shelf with the lower slope (Fig. 5). This bank seems to show a more intense dismantling by faulting processes, like the normal faults observed along the northern margin of the Puerto Rico Trench. Also, they may be a gravitationally driven block glide associated with margin collapse. There is an anomalous area in the southern edge of Navidad Bank, where GLORIA side-scan data shows a very high reflectivity ridge similar to carbonate outcrops of Navidad Bank (Mullins et al., 1992) and single-channel seismic profiles show an internal structure with many diffractions (Figs. 11 and 12). This suggests that carbonate blocks from the Navidad Bank are accreted to the base of the Insular Margin.

4.2 Hispaniola Trench Province

New bathymetric data show that the morphology of the HT is complex and is conditioned along the strike by the tectonic domains of the study area. In the OUD it is mainly represented by the Hispaniola Basin, which opens to the west to form the Caicos Basin (Fig. 3). To the east, Hispaniola Basin is interrupted by the Silver Spur and, in the OCD, the trench is formed by an alternation of small basins and carbonate spurs impinging into the IM. The axial bathymetric profile shows an alternation of high-standing carbonate spurs and small isolated basins (Fig. 13). The water depth along the isolated basins increases eastward to finally connect with the Puerto Rico Trench (8,300 m-deep; Figs.4 and 13). For a better reference and because of proximity with well-known features, these isolated basins are called in this study: Santisima Trinidad Basin and Western and Eastern Navidad basins.

4.2.1 Hispaniola and Caicos basins

The Hispaniola Basin consists mostly of a sinuous, featureless, flat-bottomed (seafloor slope <2º) elongated depression, with depths around 4,200 m (Fig. 4 and App. A). The width of the Hispaniola Basin is very variable and is conditioned by the irregular morphology of the Bahamas

spurs and the existence of wide passages between the banks. To the east, the Hispaniola Basin disappears, in the collision zone between the Silver Spur and the IM, where the water depth quickly decreases to 2,500 m (Fig. 5, App. A). It only remains a small elongated sedimentary filling less than 3 km-wide (Fig. 9). At the western part of the survey area, the basin opens and forms the extensive Caicos Basin that is bounded to the north by the Turks and Caicos Islands and to the west by the Inagua Island (Fig. 1).

The sedimentary fill of Hispaniola and Caicos basins consist of horizontal to sub-horizontal turbiditic levels with variable thickness, characterized by very reflective, continuous and little spaced reflectors (Figs. 8 and 14). Caicos Basin has a turbiditic fill with at least 2 sTWT of thickness in which can be distinguished two seismic units: a) an upper unit consisting of a package of sub-parallel, continuous and high-amplitude reflectors; and b) a lower unit consisting of a package of sub-parallel, semi-continuous and mid-amplitude reflectors (Fig. 14). GLORIA data show a long channel from Caicos Basin that flows into the western edge of Hispaniola Basin (Dillon et al., 1992). This is a very narrow area south of Mouchoir western spur with large sedimentary fill (up to 2.5 sTWT; Fig. 6) and corresponds to the deepest region of the HT (4,300 m-deep; Fig. 13 and App. A). The channel forms a sedimentary channel-levee system. Laterally, the most recent turbidite levels show an onlap with the underlying turbidite levels or with high-standing carbonates of the BCP (Figs.7, 8, 9 and 14). In the southern part of the Hispaniola and Caicos basins the turbiditic levels are progressively tilted towards the north, folded and cut-off by the N-verging thrusts and finally incorporated to the NHDB (Fig. 14). Occasionally, sedimentary reflectors from Bahamas Banks can be followed southwards below the Hispaniola Basin turbiditic filling evidencing the active underthrusting process of the banks (Fig. 8). Dolan et al. (1998) describe a carbonate basement beneath the turbidite filling, but multi-channel seismic profiles do not show enough resolution. Modern turbidite reflectors onlap an erosive surface, and below it there is an older turbidite filling characterized by discontinuous horizontal reflectors (Figs. 7, 8 and 14). The drainage systems developed on the flanks of the Bahamas

Banks and on the IM, indicate that turbidite materials come mainly from the island of Hispaniola and to a lesser extent from the BCP (Fig. 4). Several morphological elements reflect this, such as the big submarine channel NE of Cap-Haitien that flows into the Caicos Basin, forming a great submarine fan (Dillon et al., 1992). Another important sedimentary input from the island arc to the basins are the occasional mass transport deposits (MTD) that are interbedded with the turbiditic fill of both basins (Fig. 8 and Fig. 14). Widespread seafloor sampling in the Caicos Basin showed that most of the sediments come from the island arc, where these channels transport detritic materials of sand size through turbiditic flows (Ditty et al., 1977). These detritic deposits are interbedded to a lesser extent with pelagic sediments and carbonate sediments from the banks.

4.2.2 Trench basins in the Oblique Collision Domain

In the OCD the HT becomes significantly narrower and deeper than in the OUD (Fig. 5). In a segment of 200 km-long, eastwards from the Hispaniola Basin at 4,200 m-deep, the axial depth increases by means of an alternation of highs and lows up to the Puerto Rico Trench where the water depth reaches 8,300 m (Fig. 13). The highs in the axial profile correspond to carbonate spurs that impinge into the IM, and the turbiditic fill accumulated in this bathymetric trench is discontinuous (Fig. 9). The lows are occupied by elongated isolated basins which from W to E, are: Santísima Trinidad (4,400 m-deep), Western Navidad (4,600 m-deep) and Eastern Navidad (5,400 m-deep). These basins have a preferential elongated E-W morphology with variable turbiditic thickness, reaching locally 1.5-2.0 sTWT (Figs. 15 and 16). Seafloor sampling in the Santísima Trinidad Basin showed a mixture of terrigenous and carbonate turbidites derived from the IM and the carbonate banks (Seiglie et al., 1976). Below this turbiditic fill it can be inferred a stepped southward dipping carbonate basement (Figs. 11, 12 and 16). Because of the irregular trench bathymetry in the OCD the entrance sediment to the trench basins from the Bahamas Banks and the IM seems to be lesser than in the OUD. In the lower IM there is no evidence of a

drainage system feeding the Santisima Trinidad and Navidad basins. Canyon systems in the area do not flow into the trench basins, mainly since the deformation front act as an efficient sediment barrier. Widespread slumped areas might provide the greatest sedimentary inputs to Eastern Navidad Basin and the eastern end of Western Navidad Basin (Fig. 5). The drainage system developed in the slope banks seems to be a local source of carbonate sediments for the adjoining basins.

4.3. Insular Margin (IM)

The Northern Hispaniola Margin is WNW-ESE oriented, comprising from the northern Hispaniola shoreline to the base of the insular slope. This slope forms the southern wall of the HT and has two along-strike oriented morphostructural sub-provinces: The Insular Shelf and the Insular Slope (Figs. 3, 4 and 5).

4.3.1 Insular Shelf

Although the Insular Shelf sub-province is not covered by high-resolution swath bathymetry data (water depths are below 200 m), the GEBCO 30 arc-sec. gridded data allow to roughly draw the shelf edge along the margin. The shelf edge is sinuous, resulting in a variable shelf width along the margin. Although the averaged width is between 3 and 5 km, there are zones where insular shelf is almost non-existent (e.g., Manzanillo Bay and Sosua and Rio San Juan peninsulas; Fig. 3), and areas where the shelf reaches 25 km seaward from the coast (e.g., Monte Cristi; Fig. 4). The lithology of the insular shelf was inferred from onshore geological studies of northern Hispaniola (de Zoeten and Mann, 1999, and references therein). The current shelf is mainly constituted by Late Miocene-Present shallow carbonate materials built over deep-marine Eocene-Paleocene rocks with a Paleocene-Eocene volcano-sedimentary basement.

4.3.2 Insular Slope

Morphostructure

Based on morphological criteria, the Insular Slope sub-province can be divided into two along-strike regions of slope: an upper region characterized by a steep continuous slope and a lower region characterized by a highly benched and stepped slope (Fig. 3, App. C). The boundary between both regions is not always identified along-strike, but it can be outlined along a concave slope break (Figs. 4, 5 and App. C).

The lower region of the Insular Slope sub-province is occupied by the NHDB. This deformed belt consists in an alternation of roughly E-W trending broad anticline ridges and narrow troughs, sub-parallel to the base of the island slope where is located the compressive deformation front (Figs. 4 and 5). This alternation is the surface expression of a sequence of fault-propagation faults that form an imbricate fold-and-thrust system (Figs. 6-10 and 14). Although the imbricate system is composed of highly deformed sediments, folded sediment beds can be identified, forming broad anticline ridges with preferential northward vergence (i.e., steeper northern flanks and gentler southern flanks; Figs. 4, 5; App. C). Sub-surface data image the structure of the imbricate fold-and-thrust system and shows a northwards transport direction (Figs. 6 and 14). However, frequent slope failures highly alter the surface expression of the verging anticlines, mainly in the steeper northern flanks (Fig. 4, 5, 7 and 8). Significant sediment accumulation over the axial ridge zones and the gentler southern flanks, which are partially buried by syn-tectonic sediments, locally forming ponded elongated slope basins (i.e., piggy-back basins; Figs. 7, 8 and 14). These basins have variable size and sediment thickness, reaching locally 0.5 sTWT (Figs. 8 and 14). They often show fanning beds, confirming the intense active deformation during the sediment accumulation (Figs. 8 and 14). The base of the insular slope mostly coincides with the active compressive deformation front that is marked by the seaward frontal thrust fault and its associated northward-verging anticline ridge (Figs. 4-8 and 14). Most

thrust faults are buried by slope sediments (i.e., blind thrusts) and they are only inferred by the overlying verging anticline ridge, but locally they propagate upwards reaching the seafloor (Fig. 8).

The development and the surface expression of the NHDB is highly variable along the entire margin showing significant differences between the Collision and Underthrusting domains. These differences are:

a) Generally, in the OUD, the imbricate system shows a marked seafloor expression. This allows to observe the existence of individual broad anticline ridges (Fig. 4). However, the along-strike development (i.e., length) is very variable, as can be inferred attending to the number of anticline ridges and the sinuous trace of the deformation front. There are broad salients (up to 25 km seaward of width) where there is a well-developed imbricate thrust system (e.g., in the Caicos Basin region the imbricate system is built by a succession of at least 5 anticline ridges separated in average 5 km; Figs. 4 and 14) and narrow recesses where the anticline ridges are difficult to observe or simply do not exist (e.g., south of Mouchoir western spur). This alternation of salients and recesses has been interpreted in many studied imbricate thrust belts, and reproduced by analogue modeling, as a consequence of differential sediment accretion and/or the topography of the incoming plate (e.g., Scholl et al., 1980; Dominguez et al., 1995; Marshak, 2004; Granja-Bruña et al., 2009, 2014). In our instance, the sinuous morphology of the deformation front seems to be similar in origin. This is supported by the observed along-strike changes in the sediment thickness of the Hispaniola trench, as well as by the variable topography of the underthrusting BCP. Most of the NHDB is formed by one or two long and broad anticline ridges (Figs. 4, 6, 7, 8 and 14). The width of the anticline ridges does not seem to be variable, averaging 3-5 km, but their along-strike length is very variable, from only 10 km to 40 km (Fig. 4).

b) In the OCD, the surface morphology of the NHDB is very diffuse and it is only inferred upwards in the slope, through a series of 3 to 4 NW-SE trending anticline ridges (Fig. 5). The width and the length of anticline ridges are very limited in contrast to the OUD. Here, the ridges are very narrow averaging 1 km of width and their along-strike length are only up to 8 km. Downslope, the anticline ridges show a smooth surface expression since there is a relatively thick blanket of slope sediments that partially buries the low-active N-verging imbricate system (Figs. 5 and 10). This sedimentary cover shows a gentle seaward gradient, locally deformed by shallow gravity-driven failures that yield small fault scarps and a widespread slump scars (Figs. 5, 10, App. C). Locally, the deformation front incorporates carbonate material from the southern flank of the BCP (accreted carbonate block in Fig. 12). In the backside of the imbricate system, where there is a significant concave slope break, an elongated E-W trending >1 sTWT-thick slope basin is observed. In the south-eastern corner of our survey area, there are two striking E-W-trending valleys that could be left-lateral strike-slip structures probably connecting eastward with the western end of the Bunce Fault (ten Brink et al., 2004). Because of the lack of data, we cannot study the westward interconnection with the compressive structures of the NHDB in the north of the Samaná Peninsula.

The slope region located between the shelf edge and the rear of the NHDB is not fully covered by high-resolution multibeam data, but the explored areas show a rough, steep continuous and locally stepped slope that is covered by variable-thick slope sediments (Fig. 7, 8 and 14). Here, the seafloor is incised by a dense canyon network and numerous gravity-driven failures (Fig. 4, 5, 7, 8). Limited penetration of seismic data and the acoustic basement prevent the identification of any structural feature beneath this slope region (i.e., a potential buried imbricate system or island arc rocks).

Submarine drainage

The Northern Hispaniola Margin locally shows a well-developed canyon and channel network that seems to be an important sediment transport and distribution mechanism along the slope and deep basins. The network is more developed in the OUD where several large channels fed by many tributary canyons go from the shelf edge (shelf-sourced channels; Farre et al., 1983), or indeed from the onshore river mouths, through the entire margin to the abyssal plains of the Caicos and Hispaniola basins (Fig. 4). Because of the stepped slope yielded by the underlying imbricate structure, the anticline ridges act as efficient sediment traps, and locally some channels only reach the isolated slope basins. Occasionally, the flanks of the broad anticline ridges also show local incised canyon networks, which connect the uplifted anticline axis to the adjacent basins. In the western survey area, north of Cap-Haitien, there are three large channels that cross completely the imbricate structure and flow into the Caicos Basin (Fig. 4). The two western channels are very incised in the margin forming a 400-600 m-deep V-shaped valleys. These channels are headless and then disconnected from the onshore supplies by the active tectonics associated to the SFZ. The dip-slip component of displacement has created a WNW–ESE trending 200-500 m-deep valley along the upper slope that have beheaded these channels (Leroy et al., 2015). This fault-controlled valley captures all the onshore supplies in the Cap-Haitien region. The longer and wider eastern channel is also very incised, forming a 400 m-deep U-shaped valley and an important sediment accumulation along its course. Where this channel reaches the Caicos Basin seafloor, it yields an extended submarine fan (Fig. 4). This submarine fan has little geomorphic expression and cannot be detected due to the limited vertical resolution of swath bathymetry data at 4,000 m of water depth. However, it was clearly mapped from the GLORIA large-range side-scan sonar images as a region of high reflective coarse sediment (Dillon et al., 1992). The available swath bathymetry data coverage allows the recognition of this geomorphic feature up to the upper slope, but we could not discard that this channel might be related to the large onshore rivers in the region, for instance the Yaque del

Norte (Fig. 4). Anyway, these channels seem to be the main sediment supply for the Caicos Basin (Fig. 4).

The OCD shows a continuous slope having a dense canyon network that supplies sediment to a series of elongated W–E trending slope basins located in the middle slope, resulting in a significant accumulation of sediment (> 1sTWT; Figs. 5 and 10). Also, there are large sedimentary processes on the middle slope at the bottom of these great canyons (Fig. 5). The larger canyon in the area is located in the Bahía Escocesa and could be connected with important rivers (i.e., Boba and Yuna rivers; Fig. 5), but we do not have swath bathymetry coverage in the upper slope to confirm that. Channels and canyons in the area do not seem to reach the Santisima Trinidad and Navidad basins, mainly due to the deformation front, which act as an efficient sediment barrier. East of the Samaná Peninsula there is not a well-developed canyon system and drainage seems to be controlled by the two striking E-W trending valleys that could be left-lateral strike-slip structures connecting eastward with the western end of the Bunce Fault (ten Brink et al., 2004).

Gravity instabilities

Gravity features as slump scars and deposits, are frequent in the IM (Figs. 4 and 5). The size of the slope failure is variable but seems to be related with the height of the anticline ridges. For instance, in the salient of the NHDB located in the Caicos Basin, slope failures have smaller size because the anticline ridges are smaller. On the contrary, the frontal anticline ridges located south of the eastern Mouchoir Spur show a significant larger size because the anticline ridges are much wider and higher (Figs. 4 and 8). Here, in the northern flank of the frontal anticline ridge, the gravity instability coalesces resulting in an extended slumped area. Locally because of the larger size of the slumps (8.6 km-long, 7.8 km-wide), and possibly the recent activity, the slump deposits and the head scarps of 300-400 m-high are preserved (Figs. 4, 7 and 8). In the OCD, small gravity instabilities are relatively less frequent (Fig. 5), but in the lower slope zone,

there are widespread slumped areas forming a relative thick sediment fill that covers the imbricate system (Figs. 10-12). The slumped area from the east is the biggest one, covering 40 km-long along-strike and 12 km-wide downslope. In the middle slope, there is one lager slump scar near the elongate W-E slope basin (Fig. 5). This slump shows a sinuous head scarp, with minor cracks in the slumped regions, and could be associated with the over-steepening of the mid-slope in this region where there are also many gravity-driven faults.

5. Discussion

5.1. Erosion and collapse of the southeastern of Bahamas Carbonate Province

The southeastern BCP belonged once to a much larger and continuous carbonate platform that would include the present Great Bahama Bank (Mullins and Hine, 1989; Mullins et al., 1992). Latter authors suggested that the current morphology of the southeastern BCP, with large scalloped banks separated by deep passages, would be the result of at least two retreat stages of the carbonate platform: A Middle Cretaceous drowning stage related to a global response of carbonate platforms to a rapid pulse of sea level rise (Schlager, 1981; Larson and Pitman, 1972; Sheridan, 1983), and a Middle Miocene-Present underthrusting stage of the Bahamas Carbonate Province along the Northern Hispaniola Margin (Sykes et al., 1982).

The limited region of the carbonate banks covered by our data do not allow to corroborate the Middle Cretaceous drowning stage, but we have observed numerous features in the carbonate banks that can be attributed to the NOAM-CARIB boundary plate interactions since Middle Miocene times. Along the lower slope of the carbonate banks numerous recent structural and sedimentary features seem to jointly contribute to the erosional retreat of the carbonate banks:

a) The flanks of the carbonate banks show widespread local networks of incised canyons/gullies. Most small canyons and gullies show V-shaped cross-section, suggesting they are essentially

active erosive features (Shepard, 1972). Occasionally, northward of the regions covered by swath data, the GLORIA side-scan sonar data shows some large channels that connect the upper slope bank, and possibly the bank edge with the Hispaniola Basin seafloor (Figs. 4 and 5; Dolan et al., 1998). Those larger canyons show a wide U-shaped cross-section suggesting that they are the most active agents in transporting and redistributing sediments along the bank slopes up the Hispaniola Basin. The accumulation of sediments transported by canyons and channels, and likely redistributed by bottom currents can be locally recognized at the lower slope, at the base of the flanks, and along the passages. Such deposit accumulations form a hummocky seafloor morphology and the chaotic internal geometry of the sedimentary reflectors resemble to debris flows, fans and drift deposits (Figs. 8-10 and 15). Fan deposits can be recognized at the mouth of large channels over the Hispaniola basin seafloor (Fig. 4). GLORIA data also show a huge extended region of debris flows between the marginal relief and the eastern spur that seems to be related to a significant erosive process (Fig. 4; Dolan et al., 1998). Probably because of the limited vertical resolution of the swath bathymetry data, we cannot recognize some other possible deposits on the lower slope.

b) There are numerous head scarps suggesting that slumping is a widespread significant erosional process. Slump scars are mostly located nearby fault and morphologic scarps, and over recently-tilted block faults (Figs. 4, 5, 7 and 8). The mechanism of slump triggering would be 1) intrinsic, due to the over-steepening caused by active fault deformation and/or 2) extrinsic, caused by deep oceanic currents and shaking yielded by frequent and significant magnitude seismicity due to the proximity of the active plate boundary.

c) The frequency, along-strike length, and average amount of dip-slip throw of the normal fault scarps is variable along boundary plate (Figs. 6-9 and 11). In the OCD there are higher frequency and larger average amount of dip-slip throw (e.g., reaching 0.5 sTWT ≈ 350 m-high; Figs. 10 and 11) than in the OUD (Figs. 6, 7 and 8). Scarp faults are E-W trending and sub-parallel to the

convergent plate margin. This geometrical parallelism between the structures in the incoming plate and the boundary plate has been well-documented in many subduction and underthrusting settings (e.g., Jones et al., 1978; Hilde, 1983 and references therein; von Huene and Culotta, 1989). Normal faults in the incoming plate near the trench are a result of the plate bending and/or the along-strike differential overload of the trench and accreted sediments. Here, it seems that the bending of the incoming plate because of the oblique collision/underthrusting plays the most significant role, as there is no relation of a more developed thrust belt with the existence of normal faulting.

d) The preferential enlargement of the carbonate spurs with their SW-NE trending flank scarps, and the wide and deep passages separating them (the N-S trending Silver bank passage and the NE-SW trending ST and N passages) seem to be older lineal structures inherited from Early Cretaceous rifting (Mullins et al., 1992), and not directly related to the Miocene-to-present underthrusting/collision process. These passages are related to erosional reentrants north of Navidad Bank identified by Mullins et al. (1992), which are parallel to the trend of marine geomagnetic trends in the North Atlantic (Klitgord et al., 1984). This Early Cretaceous rift stage could also provide a first-order mechanism for the origin of bank segmentation and basin physiography in the southeast Bahamas (Freeman-Lynde and Ryan, 1987). Since the collision between Hispaniola margin and the Bahamas Carbonate Province, these inherited structures could act as transverse tear faults in the incoming plate. In our opinion. west of Silver Bank, the structure in the channel, could accommodate the change in the plate coupling, the amount of shortening or the stress fields between the underthrusting and collision domains suggested by Dolan et al. (1998). In the OCD, the escarpments on the flanks of the Navidad and Santisima Trinidad banks mark the boundary between the stepped trench basins and may also act as transverse tear faults, favoring the deepening the trench basins towards the E (Fig. 13).

e) Passages between banks are not filled in, as it occurs in NW BCP. In NW Bahamas, Masaferro and Eberli (1999) proposed that shortly after the Cuba-Bahamas collision, the highly productive carbonate environment (or "carbonate factory"; as defined by Schlager, 2000 and 2015) healed the depressions masking the scars produced by tectonism during the rifting stage (Middle-Upper Jurassic). After collision stage, the NW BCP works as passive margin and the sedimentation along the slopes of the banks and on the passages is continued controlled by margin collapse and deep currents (e.g., Mulder et al., 2012; Jo et al., 2015; Tournadour et al., 2015; Principaud et al., 2018). However, in SE Bahamas the collision/underthrusting process between the SE of the BCP and the island arc is still ongoing (Dolan et al., 1998 and this study). We suggest that this could drive the distinct morphology and sedimentation patterns between the NW and SW regions of the BCP. The proximity to an active plate boundary of the SE Bahamas would cause that the banks might be too deep to be effective "carbonate factories" (App A; Schlager, 2000; Schlager, 2005), preventing the healing of the passages.

5.2 Tsunamigenic sources in northern Dominican Republic

5.2.1 Sources from 1946 Bahía Escocesa tsunami

The main event of August 4th, 1946, with M8.1, was the first of a series of five major earthquakes (M>7) that struck the northern of the Hispaniola island between 1946 and 1953 (e.g., Dolan et al., 1998; Dolan and Wald, 1998). The rupture area of the main event inferred from the aftershock distribution along the boundary plate occupies the OCD between Navidad and Silver banks (Figs. 1 and 17). The oblique thrust mechanism and the shallow focal depth suggest that this event was nucleated in a highly coupled segment of the interface between the NOAM and CARIB plates (Figs. 1 and 17; Dolan et al., 1998). The 1946 main earthquake was followed by a tsunami that mainly impacted in the coastal towns of the Bahía Escocesa (Fig. 17; Lander et al., 2002 and references therein; Fritz et al., 2018). The greatest damage and loss of life occurred at the village of Matancitas (just south of the present city of Nagua, then known as

Julia Molina), where a 2.5 m-high tsunami flattened homes and buildings. Because of the low relief in most of the coastal areas, the tsunami propagated inland for several kilometers killing approximately 1,790 people (previous estimates placed the death toll near 100; Lander et al., 2002). Matancitas and nearby coastal towns were destroyed by the tsunami and abandoned. Farther north, at the mouth of Rio Boba, higher coast relief overtopped by the tsunami required tsunami heights of 4-5 m (Lynch and Bodle, 1948). The tsunami impacts peaked with maximum tsunami heights exceeding 5 m between Cabrera and El Limon (Fritz et al., 2018). A maximum tsunami height of 8m was measured in Playa Boca Nueva (Fritz et al., 2018) In the eastern termination of Bahía Escocesa, at Cabo Samaná, several ebbs and flows were observed, but no damage occurred. Tsunami inundation distances of 600 m was measured at las Terrenas and Playa Rincon on the Samaná Peninsula (Fritz et al., 2018). The wave was also recorded at San Juan (Puerto Rico), and as far as Bermuda, Daytona Beach (Florida), and Atlantic City (New Jersey). After the large tsunami, smaller tsunamis continued for several days (tidal waves; Seismological Notes, 1946). Anecdotal accounts noted that the tsunami propagated form north to south down the coast, indicating a source to the north. Considering the areas documented, the impacted area by the tsunami should be more extended in northern coast of Hispaniola, affecting to the Puerto Plata region, but there are no records.

The sources of the August 4th, 1946 large tsunami and subsequent smaller tsunamis remains unknown after several studies from seismological point of view (Heck, 1947; Lander, 1997; Dolan et al., 1998; O'Loughlin & Lander, 2003; Gailler et al., 2015; Grilli et al., 2016). Based on the places impacted by the tsunami, Dolan and Wald (1998) suggested that it was probably caused by:

a) Seafloor co-seismic rupture. Seafloor uplift associated with propagation of the mainshock rupture to the sea floor at the collisional deformation front.

b) Widespread, earthquake-induced slumping of the Hispaniola slope or the southern slopes of Silver or Navidad banks.

These hypotheses are discussed here under.

a) Seafloor co-seismic rupture hypothesis

Dolan et al. (1998), suggested that the 1946 tsunami could be caused by a seafloor co-seismic rupture. They interpreted and elongated basin slope at the base of the Samaná Peninsula slope, bounded southward by a N-dipping normal fault (the Samaná Peninsula slope is the exposed fault scarp) and northward by a S-dipping reverse faults with significant reverse strike-slip component (they named this fault as the North Hispaniola slope fault). They also suggested that the North Hispaniola slope fault curves westward into a SW orientation where it apparently controls the location of several linear submarine canyons segments. They speculated that these structures continue southwestward related with the onshore SE-facing lineal scarp southwest of Nagua (Nagua escarpment; Fig. 5), and ultimately connecting with the SFZ. They finally suggested that these structures could be the source of the tsunami. The interpretation of Dolan et al. (1998) was based on a seismic line that crosses over the head scarp of a slump located northward, and the seafloor shows an apparent vertical step (see Figs. 13A and B in Dolan et al., 1998). We have reprocessed and reinterpreted in detail the single-channel seismic lines crossing this structure, in combination with the high-resolution swath data (Figs. 10 and 16). The suggested W-E trending faults bounding southward and northward the elongated slope basin do not seem to be faults in our interpretation. Sediment reflectors do not show any drag-fold, fanning beds or any kind of kinematic markers in the basin fill. The suggested N-dipping fault is the downward continuation of the steep insular slope of the Samaná Peninsula (Fig. 10). The suggested S-dipping fault is formed by the sharp slope change between the flat seafloor of the basin and the backward limb of a fault-propagation fold structure, forming part of the imbricate system (Figs. 10 and 16). The accommodation space that allowed the formation of this basin is

related to the vertical growth of the imbricate system (e.g., Ori and Friend, 1984; Mulugeta and Koyi, 1987). In addition, swath bathymetry does not show any offset in the canyon network that could suggest a strike-slip component as proposed by Dolan et al., 1998. Westward, the northern boundary of the basin loses surface expression and is buried beneath the sediments deposited at the mouth of the large canyon system running along the steep slope from the Rio Boba (Fig. 5). The northern slope of the Samaná Peninsula is featured by a steep seafloor highly incised by the dense canyon/gully network. Most of the network seems to be developed along the maximum slope without any structural control.

In addition, our swath data do not show any evidence of a recent reverse rupture on the seafloor along the OCD. There are several elongated ridges with significant seafloor expression, but they seem to be normal faulted carbonate blocks of the Santísima Trinidad and Navidad banks (Fig. 5). Similar ridges have been described eastward in the Puerto Rico Trench and they are not related with the accretion process (ten Brink et al., 2004). However, although any surface rupture has not been identified, during the time interval since the tsunami struck the Bahia Escocesa (70 years ago), intense erosion and sedimentation processes could have blurred this feature from the seafloor. Moreover, several studies point out that a seafloor surface rupture with significant vertical motion is not necessary for tsunami generation (Iwasaki., 1982; Tanioka and Satake, 1996; Ito et al., 2011; Song et al., 2017). This is the case of the 2011 Tohoku (Ito et al., 2011; Fujiwara et al., 2011) or the 2004 Sumatra (Song et al., 2017) events, where the tsunami is originated by a large horizontal displacement of the frontal accretionary wedge. In response to this movement, the water column above the displaced wedge is pushed upwards forming the tsunami.

b) Earthquake-induced slumping hypothesis

An alternative interpretation is that the source of the 1946 tsunami was a large local or small widespread slumping. This slumping would be earthquake-induced and located in the epicentral

region of the steep slopes of the Northern Hispaniola Margin or of the Bahamas Banks (Dolan et al., 1998). In the region covered by swath data, we have identified a large slump in the mid-insular slope (Fig. 5). This slump shows a clear bathymetric expression with head and lateral scarps of 100-150 m-high, defining a slumped area of at least 35 km^2. The headscarp is facing northwestward, suggesting a flow to the NW, but there is not a recognizable slump deposit. Relatively small slumped area and distant regions affected by the wave (e.g., eastern coast of U.S.A.) suggest that this scenario is not much feasible, but further specific tsunami simulations are necessary to test this hypothesis.

In the OCD, south of Navidad Bank, there is a widespread slumped area that reaches 350 km^2. The seafloor surface of this region is irregular and prevents the identification of any structural feature that could be associated with of the NHDB (e.g., anticline ridges). This slumped region could be associated with the steep seafloor slopes and the extreme shaking yielded by the 1943-1953 seismic crisis. This doesn´t seem to be the source of the main tsunami of 1946, but could be related with the minor tsunamis documented several days after the main shock (Lynch & Bodle, 1948; Lander et al., 2002; O'Loughlin & Lander, 2003).

The steep slopes of the upper insular slope and the southern flanks of Bahamas Banks are also prone to earthquake-induce slumping. However, in the region covered with swath bathymetry, there is no any evidence of large slumping, only small slumps. These small slumps could also be the source of the post-mainshock small tsunamis recorded in the region. More studies recoding high-resolution bathymetry and side-scan sonar are necessary in the BCP (erosive flanks) and in the upper Hispaniola slope to identify the source, as well as tsunami modeling with different scenarios to reproduce the observed tsunami run-up and impacted areas.

5.2.2 Other tsunamigenic sources along the margin

Other potential sources of tsunami in the northern coast of Hispaniola would be related to the active tectonics along the OUD of the NHDB. In 1994 and 2003 several remarkable events with

M5.0 and 6.3 respectively occurred offshore near Puerto Plata, the most populated city in the northern coast of Hispaniola (Dolan and Bowman, 2004). The main event of 2003 triggered a seismic crisis with a significant M5.6 aftershock one hour later, and numerous smaller aftershocks for more than a month. 1994 and 2003 events have similar shallow focal depths (≈15 km) and pure thrust fault mechanisms with a nodal plane near vertical and another gently S-dipping (Fig. 1). These mechanisms were interpreted as thrust fault displacements in the NHDB accommodating the oblique convergence at the interplate surface of the underthrusting domain or to large thrusts faults in the NHDB (Dolan and Bowman, 2004). Although seismic data do not allow imaging the detachment interface, several large thrust faults have been identified along the NHDB (Fig. 4). Thrust faults can be outlined almost to the sea surface suggesting they can reach the seafloor surface. If the main seismic events yield a co-seismic rupture that propagates upwards, then there will be a sudden seafloor uplift with significant tsunamigenic potential. On the other hand, the continuous non-seismic deformation in the NHDB resulting in the growing of the anticline ridges yields over-steeping of the seafloor slope. This circumstance is favourable for gravitational slumping that also can be triggered by the shook of the seismic events. The NHDB north of Puerto Plata has numerous gravity slumps, some of them of large size. The larger and more abundant gravitational instabilities are found in the steeper forward limb of the frontal anticline ridge (Fig. 4). Evidence supporting this slumping process is a recurrent process can be found in the mass transport deposits (MTD) identified in the Hispaniola and Caicos basin turbiditic fill (Figs. 8 and 14). It seems highly probable that some of these instabilities have been triggered by earthquakes, and although no tsunamis have been documented, their analysis and possible impact on future events should be considered (McCann, 2006).

6. Summary and Conclusions

A combined interpretation of high-resolution swath bathymetry and 2D seismic reflection data, together with published GLORIA side-scan sonar data, have allowed us to characterize, on a regional scale, the active sedimentary and tectonic processes in the Dominican sector of the NOAM-CARIB plate boundary. Three along-strike morphostructural provinces have been identified: a) the Bahamas Carbonate Province, b) the Hispaniola Trench and c) the Insular Margin. However, because of the high oblique plate interaction, those provinces show major along-strike differences in the active sedimentary and deformational processes, related to two distinct tectonic domains respectively: Oblique Underthrusting and Oblique Collision domains located in the western and eastern regions of the surveyed area respectively.

Bahamas Carbonate Province

The southeastern end of BCP has many inter-related morphological and structural features suggesting active erosional and deformational processes. The result is a widespread collapse and retreat of the carbonate banks that seems to increase close to the active boundary plate (c.f., northwestern BCP; Sheridan et al., 1988). The southern flank of the banks shows frequent normal fault escarpments sub-parallel to the NOAM-CARIB plate boundary that seem to be consistent with a crustal flexure and subsidence related to the underthrusting and collision processes. Slope processes (i.e., slumping, debris flows and canyon systems) show more occurrence related to morphological and fault-controlled scarps.

Hispaniola Trench

In the OUD, the Hispaniola Trench is characterized by two large flat-bottomed intercommunicated basins with water depths averaging 4,200-4,300 m: Hispaniola and Caicos basins. Basin turbidite thickness is substantial along the strike, locally reaching 2.5-3.0 sTWT, suggesting high accommodation space yielded by the boundary plate interaction. In the OCD, the HT is segmented and comprises a 200 km-long area consisting of elongated E-W trending

basins separated by bathymetric highs that correspond to carbonate spurs. The depth increases to the east, from 4,400 m-deep in Santisima Trinidad Basin to 8,300 m-deep of Puerto Rico Trench. This fill is lying over southward dipping carbonate basement from the banks.

Insular Margin

In the OUD the NHDB forms a NW-SE trending N-verging fold-and-thrust imbricate system mainly affecting the accreted turbidites of the Hispaniola Trench. The development of the imbricate systems is variable along-strike having an alternation of broad salients, with several anticline ridges, and narrow recesses where only a frontal thrust is recognizable. These along-strike variations seem to be related with the differential topography of the incoming NOAM plate. Slope processes are also common seafloor features in NHDB but highly controlled by the active imbricate system. Slumping is mainly concentrated in the steeper northern flanks of the anticline ridges. Tough slumps commonly have a small size, four large slumps are also identified in the frontal anticline ridges. The canyon system networks are small and controlled by the stepped bathymetry of the imbricate system, and then they are the only sediment contributors for the small slope basins. However, locally three large channels by-pass the Insular Margin Province and connects the Insular Shelf with the trench basins, forming huge depositional systems (e.g., large submarine fan in the Caicos Basin). In the OCD, the Insular Margin Province presents a smooth seafloor morphology, only with few distinguishable features. Most part of the Insular Slope sub-province shows a relatively thick slope sediment cover that is burying a low active and diffuse N-verging imbricate system. Locally, the deformation front contains carbonate accreted blocks. This shows that small blocks of the southern flank of the banks are being accreted into the deformed belt during the active collision process. In the rear of the imbricate system there is an elongated E-W trending slope basin interpreted by Dolan et al., 1998, as a basin controlled by two oblique strike-slip faults. New high-resolution bathymetry data and a review of vintage single-channel seismic data do not show any evidence on the

seafloor or in sediment reflectors indicating the existence of these structures or their transpressive behavior. The formation of this basin is only caused by vertical growth of the imbricate system. In the eastern corner of OCD, there are two striking E-W trending valleys that could be left-lateral strike-slip structures connecting eastward with the western end of the Bunce Fault (ten Brink et al., 2004). Slumping processes are frequent in the OCD, forming widespread slumped areas that covers the imbricate system.

Tsunamigenic sources

Our interpretation of the active erosional and deformational features has allowed us to discuss possible tsunamigenic sources, related to the historical records that must be considered in future tsunami hazard assessments. Some of these potential sources are active thrust faults of the NHDB imbricate system that locally reach the seafloor surface. In addition, the active growth of the anticline ridges increases the seafloor gradient, contributing to the development of gravitational instabilities, some of them of significant size. These potential tsunamigenic sources have been linked to instrumental seismic events that affected the northern coastal areas of the Dominican Republic.

Because of focal solution of the 1946 main event and the documented inundation areas, we suggest that the Bahía Escocesa tsunami is related with a large co-seismic slip on the plate interface (i.e., main thrust) or on some subsidiary thrust of the buried imbricate system. However, we have not found any evidence of seafloor rupture in the epicentral area. On the other hand, widespread slumped area on the lower slop could be responsible of the small tsunamis that struck the coast in the subsequent days. The 1994 and 2003 seismic events north of Puerto Plata are related to the active underthrusting process and have been associated with thrust faults of the NHDB. These events can give as possible tsunamigenic sources those co-seismic ruptures of thrust of the NHDB that reach the surface of the seafloor or by non-seismic deformation in the NHDB, resulting in the vertical growing of the anticlinal ridges yielding the

over-steeping of the flanks, favoring the occurrence of slumps that could be triggered during a seismic event.

Therefore, earthquakes themselves cannot be the only tsunamigenic source, but also large submarine landslides or zones of major slumps triggered by the shook of seismic events may have produced them. Gravitational instabilities found on the Island Margin, mainly in the NHDB along with the development and vertical growth of the imbricate system are the two main drivers for the assessment of the seismic potential and tsunami hazards of the region.

7. Data Availability

GEBCO Digital Atlas with a 30 arc-second of resolution and onshore data has been obtained from the SRTM mission with a 90 m of resolution datasets can be found at https://www.gebco.net (General Bathymetric Chart of the Oceans, an open online bathymetric data) and at https://www2.jpl.nasa.gov/srtm respectively.

The 2D single- and multi-channel seismic reflection data, from the MW8908 (1989) and FM0503 (1980) cruises, were respectively provided by The National Oceanographic and Atmospheric Administration-National Centers for Environmental Information (www.ngdc.noaa.gov) and the Academic Seismic Portal managed by University of Texas-Institute for Geophysics (http://www-udc.ig.utexas.edu/sdc/).

Swath bathymetry data from NORCARIBE (2013) cruise cannot be shared at this time due to first author ongoing PhD studies.

Acknowledgements

We are indebted to the crew and technicians of the R/V Sarmiento de Gamboa and the Dominican patrol vessel Orion for their professional help at sea. The professional work of the technicians of the Unidad de Tecnología Marina is greatly appreciated. A. Rodriguez-Zurrunero was supported by a PhD. grant from Universidad Complutense de Madrid (CT45/15 - CT46/15). This work was also funded by CARESOIL project (S2013/MAE-2739).

References

Ali, S.T., Freed, A.M., Calais, E., Manaker, D.M., Mccann, W.R., 2008. Coulomb stress evolution in Northeastern Caribbean over the past 250 years due to coseismic, postseismic and interseismic deformation. Geophys. J. Int. 174, 904–918. https://doi.org/10.1111/j.1365-246X.2008.03634.x

Andrews, B.D., ten Brink, U.S., Danforth, W.W., Chaytor, J.D., Granja-Bruña, J.L., Llanes, P., Carbó-Gorosabel, A., 2014. Bathymetric Terrain Model of Puerto Rico Trench and the Northeast Caribbean Region for Marine Geological Investigations. U.S. Geological Survey. Open-File Report 2013e1125. http://pubs. usgs.gov/of/2013/1125/.

Benford, B., Demets, C., Calais, E., 2012. GPS estimates of microplate motions, northern Caribbean: Evidence for a Hispaniola microplate and implications for earthquake hazard. Geophys. J. Int. 191, 481–490. https://doi.org/10.1111/j.1365-246X.2012.05662.x

Bush, D.M., and Young, R., 2009. Coastal features and processes, in Young, R., and Norby, L., Geological Monitoring: Boulder, Colorado, Geological Society of America, p. 47–67, doi: 10.1130/2009.monitoring(03).

Calais, E., Freed, A., Mattioli, G., Amelung, F., Jónsson, S., Jansma, P., Hong, S.H., Dixon, T., Prépetit, C., Momplaisir, R., 2010. Transpressional rupture of an unmapped fault during the 2010 Haiti earthquake. Nat. Geosci. 3, 794–799. https://doi.org/10.1038/ngeo992

Calais, E., Mazabraud, Y., Mercier de Lépinay, B., Mann, P., Mattioli, G., Jansma, P., 2002. Strain partitioning and fault slip rates in the northeastern Caribbean from GPS measurements. Geophys. Res. Lett. 29, 3-1-3–4. https://doi.org/10.1029/2002GL015397

Calais, É., Symithe, S., Mercier de Lépinay, B., Prépetit, C., 2016. Plate boundary segmentation in the northeastern Caribbean from geodetic measurements and Neogene geological observations. Comptes Rendus - Geosci. 348, 42–51. https://doi.org/10.1016/j.crte.2015.10.007

Chalas-Jimenez, J. A., 1989. Probabilidad de un sismo catastrófico en la República Dominicana: Historia sísmica, predicción, y magnitudes esperadas (Probability of a catastrophic earthquake in the Dominican Republic: Earthquake history, prediction, and expected magnitudes): Revista Geofisica (Instituto de Geografia e Historia), v. 31, p. 185–203.

Chiocci, F.L., Cattaneo, A., Urgeles, R., 2011. Seafloor mapping for geohazard assessment: State of the art. Mar. Geophys. Res. 32, 1–11. https://doi.org/10.1007/s11001-011-9139-8

Christeson, G., Shipley, T., Gahagan, L., Johnson, K., and Davis, M., 2017. Academic Seismic Portal (ASP) at UTIG. University of Texas Institute for Geophysics. http://wwwudc. ig.utexas.edu/sdc/.

DeMets, C., Jansma, P.E., Mattioli, G.S., Dixon, T.H., Farina, F., Bilham, R., Calais, E., Mann, P., 2000. GPS geodetic constraints on Caribbean-North America plate motion. Geophys. Res. Lett. 27, 437–440. https://doi.org/10.1097/00003226-200101000-00021

de Zoeten, R and Mann, P., 1999. Cenozoic El Mamey Group of northern Hispaniola: A sedimentary record of subduction, collisional and strike-slip events within the North America-Caribbean plate boundary zone. 247-286.

Diaz de Neira, J.A., Braga, J.C., Perez Cerdan, F., Lopera, E., 2017. Las Terrazas marinas del Promontorio de Cabrera (Pleistoceno, norte de la República Dominicana). Boletín Geológico y Minero, 128 (3): 657-674. ISSN:0366-0176. DOI:10.21701/bolgeomin.128.3.007

Dillon, W.P., Austin, J.A., Scanlon, K.M., Terence Edgar, N., Parson, L.M., 1992. Accretionary margin of north-western Hispaniola: morphology, structure and development of part of the northern Caribbean plate boundary. Mar. Pet. Geol. 9. https://doi.org/10.1016/0264-8172(92)90005-Y

Dillon, W. P., Edgar, N. T., Scanlon, K. M., Coleman, D. F., 1996. A review of the tectonic problems or the strike-slip northern Boundary of the Caribbean plate and examination by GLORIA, in Gardner, J. V., Field, M. E., Twichel, D. C., (Eds.). Geology of the United States Seafloor: The view from GLORIA: United Kingdom, Cambridge University Press, 9: 135-164.

Ditty, P.S., Harmon, C.J., Pilkey, O.H., Ball, M.M., Richardson, E.S., 1977. Mixed terrigenous-Carbonate sedimentation in the Hispaniola-Caicos turbidite basin. Mar. Geol. 24, 1–20. https://doi.org/10.1016/0025-3227(77)90012-3

Dolan, J.F., Bowman, D.D., 2004. Tectonic and Seismologic Setting of the 22 September 2003, Puerto Plata, Dominican Republic Earthquake: Implications for Earthquake Hazard in Northern Hispaniola. Seismol. Res. Lett. 75, 587–597.

Dolan, J.F., Mullins, H.T., Wald, D.J., 1998. Active tectonics of the north-central Caribbean; oblique collision, strain partitioning, and opposing subducted slabs, Active strike-slip and collisional tectonics of the northern Caribbean Plate boundary zone. ISBN: 0813723264

Dolan, J.F., Wald, D.J., 1998. The 1943-1953 north-central Caribbean earthquakes: Active tectonic setting, seismic hazards, and implications for Caribbean-North America plate motions. Geol. Soc. Am. Spec. Pap. 326, 143–169.

Dominguez, S., Malavieille, J., Lallemand, S.E., 2000. Deformation of accretionary wedges in response to seamount subduction: Insights from sandbox experiments. Tectonics 19, 182–196. https://doi.org/10.1029/1999TC900055

Eberli, G.P., Ginsburg, R.N., 1987. Segmentation and coalescence of Cenozoic carbonate platforms, northwestern Great Bahama Bank. Geology 15, 75–79. https://doi.org/10.1130/0091-7613(1987)15<75:SACOCC>2.0.CO;2

Farr, T.G., Rosen, P.A., Caro, E., Crippen, R., Duren, R., Hensley, S., Kobrick, M., Paller, M., Rodriguez, E., Roth, L., Seal, D., Shaffer, S., Shimada, J., Umland, J., Werner, M., Oskin, M., Burbank, D., Alsdorf, D.E., 2007. The shuttle radar topography mission. Rev. Geophys. 45. https://doi.org/10.1029/2005RG000183

Farre, J.A., McGregor, B.A., Ryan, W.B.F., Robb, J.M., 1983. Breaching the shelfbreak: Passage from youthful to mature phase in submarine canyon evolution, in: The Shelfbreak. pp. 25–39. https://doi.org/10.2110/pec.83.06.0025

Freeman-Lynde, R.P., Ryan, W.B.F., 1987. Subsidence history of the Bahama Escarpment and the nature of the crust underlying the Bahamas. Earth Planet. Sci. Lett. 84, 457–470. https://doi.org/10.1016/0012-821X(87)90010-0

Fritz, H.M., Martinez, C., Salado, J., Rivera, W., and Duarte, L., 2017. 1946 Dominican Republic Tsunami: Field Survey based on Eyewitness interviews. 19th EGU General Assembly, EGU2017, Viena, Austria., p.11429.

Fujiwara, T., Kodaira, S., No, T., Kaiho, Y., Takahashi, N., Kaneda, Y., 2011. The 2011 Tohoku-Oki earthquake: Displacement reaching the trench axis. Science, 334, 1240, https://doi.org/10.1126/science.1211554

Gailler, A., Calais, E., Hébert, H., Roy, C., Okal, E., 2015. Tsunami scenarios and hazard assessment along the northern coast of Haiti. Geophys. J. Int. 203, 2287–2302. https://doi.org/10.1093/gji/ggv428

González de Vallejo, L. I., Ferrer, M., 2011. Geological Engineering. CRC Press/Balkema, The Netherlands, pp 678.

Granja Bruña, J.L., Carbó-Gorosabel, A., Llanes Estrada, P., Muñoz-Martín, A., ten Brink, U.S., Gómez Ballesteros, M., Druet, M., Pazos, A., 2014. Morphostructure at the junction between the Beata ridge and the Greater Antilles island arc (offshore Hispaniola southern slope). Tectonophysics 618, 138–163. https://doi.org/10.1016/j.tecto.2014.02.001

Granja Bruña, J.L., ten Brink, U.S., Carbó-Gorosabel, A., Muñoz-Martín, A., Gómez Ballesteros, M., 2009. Morphotectonics of the central Muertos thrust belt and Muertos Trough (northeastern Caribbean). Mar. Geol. 263, 7–33. https://doi.org/10.1016/j.margeo.2009.03.010

Grilli, S.T., Grilli, A.R., David, E., Coulet, C., 2016. Tsunami hazard assessment along the north shore of Hispaniola from far- and near-field Atlantic sources. Nat. Hazards 82, 777–810. https://doi.org/10.1007/s11069-016-2218-z

Hilde, T.W.C., 1983. Sediment subduction versus accretion around the pacific. Tectonophysics 99, 381–397. https://doi.org/10.1016/0040-1951(83)90114-2

Hough, G., Green, J., Fish, P., Mills, A., Moore, R., 2011. A geomorphological mapping approach for the assessment of seabed geohazards and risk. Mar. Geophys. Res. 32, 151–162. https://doi.org/10.1007/s11001-010-9111-z

IOC. Intergovernmental Oceanographic Commission, 2013. Earthquake and tsunami hazard in Northern Haiti: historical events and potential sources. Meeting of experts Port-au-Prince. UNESCO, pp. 34 (IOC/2013/WR/255).

IOC. Intergovernmental Oceanographic Commission, 2016. Sources of tsunamis in the Caribbean with possibility to impact the southern coast of the Dominican Republic, Santo Domingo. UNESCO, pp.36. (IOC/2016/WR/276 Rev.)

Ito, Y., T. Tsuji, Y. Osada, M. Kido, D. Inazu, Y. Hayashi, H. Tsushima, R. Hino, and H. Fujimoto, 2011. Frontal wedge deformation near the source region of the 2011 Tohoku-Oki earthquake, Geophys. Res. Lett., 38, L00G05, doi: 10.1029/2011GL048355.

Iwasaki, S., 1982. Experimental study of a tsunami generated by a horizontal motion of a sloping bottom, Bull. Earthq. Res. Inst. Univ. Tokyo, 57, 239–262.

James, N. P., and Kendall, A. C., 1992. Introduction to carbonate and evaporite facies models. In Walker, R. G., and James, N. P. (eds.), Facies Models – Response to Sea Level Change. St. John's: Geological Society of Canada, pp. 265–275.

Jansma, P.E., Mattioli, G.S., 2005. GPS results from Puerto Rico and the Virgin Islands: Constraints on tectonic setting and rates of active faulting, in: Special Paper 385: Active Tectonics and Seismic Hazards of Puerto Rico, the Virgin Islands, and Offshore Areas. pp. 13–30. https://doi.org/10.1130/0-8137-2385-X.13

Jansma, P.E., Mattioli, G.S., Lopez, A., DeMets, C., Dixon, T.H., Mann, P., Calais, E., 2000. Neotectonics of Puerto Rico and the Virgin Islands, northeastern Caribbean, from GPS geodesy. Tectonics. https://doi.org/10.1029/1999TC001170

Jo, A., Eberli, G.P., Grasmueck, M., 2015. Margin collapse and slope failure along southwestern Great Bahama Bank. Sediment. Geol. 317, 43–52. https://doi.org/10.1016/J.SEDGEO.2014.09.004

Jones, G., Hilde, T. W., Sharman, G., Agnew, D.., 1978. Fault Patterns in Outer Trench Walls and their Tectonic Significance, Journal of Physics of the Earth. https://doi.org/10.4294/jpe1952.26.Supplement_S85

Keefer, D.K., 1984. Landslides caused by earthquakes. Geol. Soc. Am. Bull., 95: 406-421. https://doi.org/10.1016/0013-7952(89)90044-6

Kelleher, J., Sykes, L., Oliver, J., 1973. Possible criteria for predicting earthquake locations and their application to major plate boundaries of the Pacific and the Caribbean. J. Geophys. Res. 78, 2547. https://doi.org/10.1029/JB078i014p02547

Kennet, J.P., 1982. Marine Geology. Prentice-Hall, 813 p. ISBN: 0135569362, 9780135569368

Klitgord, K.D., Popenoe, P., Schouten, H., 1984. Florida: A jurassic Transform Plate Boundary. J. Geophys. Res. 89, 7753–7772. https://doi.org/10.1029/JB089iB09p07753

Kvalstad, T.J., 2007. What is the Current "Best Practice" in Offshore Geohazard Investigations? A State-of-the-Art Review, in: Offshore Technology Conference. https://doi.org/10.4043/18545-MS

Lander, J.F., Whiteside, L.S., Lockridge, P.A., 2002. A brief history of tsunamis in the Carribean Sea. Sci. Tsunami Hazards 20, 57–94.

Larson, R.L., Pitman, W.C., 1972. World-wide correlation of mesozoic magnetic anomalies, and its implications. Bull. Geol. Soc. Am. 83, 3645–3662. https://doi.org/10.1130/0016-7606(1972)83[3645:WCOMMA]2.0.CO;2

Leroy, S., Ellouz-Zimmermann, N., Corbeau, J., Rolandone, F., de Lépinay, B.M., Meyer, B., Momplaisir, R., Granja Bruña, J.L., Battani, A., Baurion, C., Burov, E., Clouard, V., Deschamps, R., Gorini, C., Hamon, Y., Lafosse, M., Leonel, J., Le Pourhiet, L., Llanes Estrada, P., Loget, N., Lucazeau, F., Pillot, D., Poort, J., Tankoo, K.R., Cuevas, J.L., Alcaide, J.F., Jean Poix, C., Muñoz-Martin, A., Mitton, S., Rodriguez, Y., Schmitz, J., Seeber, L., Carbo-

Gorosabel, A., Muñoz, S., 2015. Segmentation and kinematics of the North America-Caribbean plate boundary offshore Hispaniola. Terra Nov. 27, 467–478. https://doi.org/10.1111/ter.12181

López-Venegas, A.M., ten Brink, U.S., Geist, E.L., 2008. Submarine landslide as the source for the October 11, 1918 Mona Passage tsunami: Observations and modeling. Mar. Geol. 254, 35–46. https://doi.org/10.1016/j.margeo.2008.05.001

Lynch, J.J., Bodle, R.R., 1948. The Dominican earthquake of august, 1946. Bull. Seismol. Soc. Am. 38, 1–17.

Manaker, D.M., Calais, E., Freed, A.M., Ali, S.T., Przybylski, P., Mattioli, G., Jansma, P., Prépetit, C., De Chabalier, J.B., 2008. Interseismic plate coupling and strain partitioning in the Northeastern Caribbean. Geophys. J. Int. 174, 889–903. https://doi.org/10.1111/j.1365-246X.2008.03819.x

Mann, P., Calais, E., Huerfano, V., 2004. Earthquake shakes “Big Bend” Region of North AmericaCaribbean Boundary Zone. Eos, Trans. Am. Geophys. Union 85, 77. https://doi.org/10.1029/2004EO080001

Mann, P., Calais, E., Ruegg, J.C., DeMets, C., Jansma, P.E., Mattioli, G.S., 2002. Oblique collision in the northeastern Caribbean from GPS measurements and geological observations. Tectonics 21. https://doi.org/10.1029/2001TC001304

Mann, P., Taylor, F.W., Edwards, R.L., Ku, T.L., 1995. Actively evolving microplate formation by oblique collision and sideways motion along strike-slip faults: An example from the northeastern Caribbean plate margin. Tectonophysics 246, 1–69.

Masaferro, J.L., Eberli, G.P., 1999. Chapter 7 Jurassic-cenozoic structural evolution of the southern great Bahama bank. Sediment. Basins World 4, 167–193. https://doi.org/10.1016/S1874-5997(99)80041-0

Marshak, S., 2004. Salients, Recesses, Arcs, Oroclines, and Syntaxes — A Review of Ideas Concerning the Formation of Map-view Curves in Fold-thrust Belts. Thrust tectonics Hydrocarb. Syst. AAPG Mem. 82 82, 131–156.

McCann, W.R., 2006. Estimating the threat of tsunamigenic earthquakes and earthquake induced-landslide tsunamis in the Caribbean, in: Caribbean Tsunami Hazard. pp. 43–65.

Mulder, T., Ducassou, E., Eberli, G.P., Hanquiez, V., Gonthier, E., Kindler, P., Principaud, M., Fournier, F., Léonide, P., Billeaud, I., Marsset, B., Reijmer, J.J.G., Bondu, C., Joussiaume, R., Pakiades, M., 2012. New insights into the morphology and sedimentary processes along the western slope of Great Bahama Bank. Geology 40, 603–606.

Mullins, H.T., Breen, N., Dolan, J., Wellner, R.W., Petruccione, J.L., Gaylord, M., Andersen, B., Melillo, A.J., Jurgens, A.D., Orange, D., 1992. Carbonate platforms along the southeast Bahamas-Hispaniola collision zone. Mar. Geol. 105, 169–209. https://doi.org/10.1016/0025-3227(92)90188-N

Mullins, H.T., Hine, A.C., 1989. Scalloped bank margins: beginning of the end for carbonate platforms? Geology 17, 30–33. https://doi.org/10.1130/0091-7613(1989)017<0030:SBMBOT>2.3.CO;2

Mulugeta, G., Koyi, H., 1987. Three-dimensional geometry and kinematics of experimental piggyback thrusting. Geology 15, 1052–1056. https://doi.org/10.1130/0091-7613(1987)15<1052:TGAKOE>2.0.CO;2

O'loughlin, K.F., Lander, J.F., 2003. Caribbean Tsunamis, Climate Change 2013 - The Physical Science Basis. https://doi.org/10.1007/978-94-017-0321-5

Obelcz, J., Brothers, D., Chaytor, J., Brink, U. ten, Ross, S.W., Brooke, S., 2014. Geomorphic characterization of four shelf-sourced submarine canyons along the U.S. Mid-Atlantic

continental margin. Deep. Res. Part II Top. Stud. Oceanogr. 104, 106–119. https://doi.org/10.1016/j.dsr2.2013.09.013

Okal, E.A., Synolakis, C.E., Uslu, B., Kalligeris, N., Voukouvalas, E., 2009. The 1956 earthquake and tsunami in Amorgos, Greece, in: Geophysical Journal International. pp. 1533–1554. https://doi.org/10.1111/j.1365-246X.2009.04237.x

Ori, G.G., Friend, P.F., 1984. Sedimentary basins formed and carried piggyback on active thrust sheets. Geology 12, 475–478.

Pacheco, J.F., Sykes, L.R., 1992. Seismic moment catalog of large shallow earthquakes, 1900 to 1989. Bull. Seismol. Soc. Am. 82, 1306–1349. https://doi.org/10.1130/0091-7613(2001)029<0347:TDFMEE>2.0.CO;2

Pérez-Estaún, A., Hernaiz Huerta, P.P., Lopera, E., Joubert, M., Escuder Viruete, J., Díaz de Neira, A., Monthel, J., García-Senz, J., Ubrien, P., Contreras, F., Bernárdez, E., Stein, G., Deschamps, I., García-Lobón, J.L., Ayala, C., 2007. Geología de la República Dominicana: De la construcción de arco-isla a la colisión arco-continente. Bol. Geol. y Min. 118, 157–174.

Pindell, J.L., Barrett, S.F., 1990. Geological evolution of the Caribbean region; A Plate tectonic perspective. Geol. North Am. https://doi.org/n/a

Pratson, L.F., Coakley, B.J., 1996. A model for the headward erosion of submarine canyons induced by downslope-eroding sediment flows. Bull. Geol. Soc. Am. 108, 225–234. https://doi.org/10.1130/0016-7606(1996)108<0225:AMFTHE>2.3.CO;2

Prentice, C.S., Mann, P., Peña, L.R., Burr, G., 2003. Slip rate and earthquake recurrence along the central Septentrional fault, North American-Caribbean plate boundary, Dominican Republic. J. Geophys. Res. Solid Earth 108. https://doi.org/10.1029/2001JB000442

Principaud, M., Mulder, T., Hanquiez, V., Ducassou, E., Eberli, G., Chabaud, L., Borgomano, J., 2017. Recent morphology and sedimentary processes along the western slope of Great Bahama Bank (Bahamas). Sedimentology. https://doi.org/10.1111/ijlh.12426

Russo, R.M., Villasenor, A., 1995. The 1946 Hispaniola earthquakes and the tectonics of the North America-Caribbean plate boundary zone, northeastern Hispaniola. J. Geophys. Res. 100, 6265–6280. https://doi.org/10.1029/94JB02599

Scherer, J., 1912. Great earthquakes in the Island of Haiti. Bull. Seismol. Soc. Am. 2, 161–180.

Schlager, W., 1981. The paradox of drowned reefs and carbonate platforms. Geol. Soc. Am. Bull. 92, 197. https://doi.org/10.1130/0016-7606(1981)92<197:TPODRA>2.0.CO;2

Schlager, W., 2000. Sedimentation rates and growth potential of tropical, cool-water and mud-mound carbonate systems. In Insalaco, E., Skelton, P. W., and Palmer, T. J. (eds.), Carbonate Platform Systems: Components and Interactions. London: The Geological Society, pp. 217–227. https://doi.org/10.1144/GSL.SP.2000.178.01.14

Schlager, W., 2005. Carbonate Sedimentology and Sequence Stratigraphy. Tulsa: SEPM (Society for Sedimentary Geology). SEPM Concepts in Sedimentology and Paleontology, Vol. 8. 200 pp.

Scholl, D.W., Von Huene, R., Vallier, T.L., Howell, D.G., 1980. Sedimentary masses and concepts about tectonic processes at underthrust ocean margins (subduction). Geology 8, 564–568. https://doi.org/10.1130/0091-7613(1980)8<564:SMACAT>2.0.CO

Seiglie, G.A., Froelich, P.N., Pilkey, O.H., 1976. Deep-sea sediments of Navidad Basin: correlation of sand layers. Deep. Res. Oceanogr. Abstr. 23, 89–101. https://doi.org/10.1016/0011-7471(76)90811-1

Shepard, F.P., 1972. Submarine canyons. Earth-Science Rev. 8, 1–12. https://doi.org/http://dx.doi.org/10.1016/0012-8252(72)90032-3

Sheridan, R.E., 1983. Phenomena of pulsation tectonics related to the breakup of the eastern north American continental margin. Dev. Geotecton. 19, 169–185. https://doi.org/10.1016/B978-0-444-42198-2.50017-1

Song, Y.T., Mohtat, A., Yim, S.C., 2017. New insights on tsunami genesis and energy source. J. Geophys. Res. Ocean. 122, 4238–4256. https://doi.org/10.1002/2016JC012556Sykes, L.R., McCann, W.R., Kafka, A.L., 1982. Motion of Caribbean plate during last 7 million years and implications for earlier Cenozoic movements. J. Geophys. Res. Solid Earth 87, 10656–10676. https://doi.org/10.1029/JB087iB13p10656

Synolakis, C.E., Bardet, J.-P., Borrero, J.C., Davies, H.L., Okal, E.A., Silver, E.A., Sweet, S., Tappin, D.R., 2002. The slump origin of the 1998 Papua New Guinea Tsunami. Proc. R. Soc. A Math. Phys. Eng. Sci. 458, 763–789. https://doi.org/10.1098/rspa.2001.0915

Tanioka, Y., Satake, K., 1996. Tsunami generation by horizontal displacement of ocean bottom. Geophys. Res. Lett. 23(8), 861–864. https://doi.org/10.1029/96GL00736

ten Brink, U., Lin, J., 2004. Stress interaction between subduction earthquakes and forearc strikeslip faults: Modeling and application to the northern Caribbean plate boundary. J. Geophys. Res. Solid Earth 109, 1–15. https://doi.org/10.1029/2004JB003031

Ten Brink, U.S., Bakun, W.H., Flores, C.H., 2011. Historical perspective on seismic hazard to Hispaniola and the northeast Caribbean region. J. Geophys. Res. Solid Earth 116. https://doi.org/10.1029/2011JB008497

Ten Brink, U.S., López-Venegas, A.M., 2012. Plate interaction in the NE Caribbean subduction zone from continuous GPS observations. Geophys. Res. Lett. 39. https://doi.org/10.1029/2012GL051485

Tournadour, E., Hanquiez, V., Ducassou, E., Gillet, H., 2015. Origin and architecture of a Mass Transport Complex on the northwest slope of Little Bahama Bank (Bahamas): Relations

between off-bank transport, bottom current sedimentation and submarine landslides. Sediment. Geol. 317, 9–26. https://doi.org/10.1016/J.SEDGEO.2014.10.003

Van Benthem, S., Govers, R., Wortel, R., 2014. What drives microplate motion and deformation in the northeastern Caribbean plate boundary region? Tectonics 33, 850–873. https://doi.org/10.1002/2013TC003402

Von Hillebrandt-Andrade, C., 2013. Minimizing Caribbean tsunami risk. Science (80). https://doi.org/10.1126/science.1238943

Von Huene, R., Culotta, R., 1989. Tectonic erosion at the front of the Japan Trench convergent margin. Tectonophysics 160, 75–90. https://doi.org/10.1016/0040-1951(89)90385-5

Weatherall, P., Marks, K.M., Jakobsson, M., Schmitt, T., Tani, S., Arndt, J.E., Rovere, M., Chayes, D., Ferrini, V., Wigley, R., 2015. A new digital bathymetric model of the world's oceans. Earth Sp. Sci. 2, 331–345. https://doi.org/10.1002/2015EA000107

Yamada, Y., Kawamura, K., Ikehara, K., Ogawa, Y., Urgeles, R., Mosher, D., Chaytor, J., Strasser, M., 2012. Submarine Mass Movements and Their Consequences, in: Yamada, Y., Kawamura, K., Ikehara, K., Ogawa, Y., Urgeles, R., Mosher, D., Chaytor, J., Strasser, M. (Eds.), Submarine Mass Movements and Their Consequences. Springer Netherlands, Dordrecht, pp. 1–12.

Figure Captions

Fig. 1 Tectonic setting of Hispaniola and surrounding regions. The red line shows the plate boundary between Caribbean plate (CARIB) and North American plate (NOAM). The black arrow indicates the plate convergence direction of NOAM relative to CARIB. The blue dashed line shows the study region. Beach balls show focal mechanisms corresponding to the 1946 mainshock and aftershocks. Red beach ball shows the 1946 mainshock focal mechanism by Russo and Villaseñor, 1995. Blue beach ball shows the 1946 mainshock focal mechanism by Dolan et al., 1998. Green beach balls show the 1994 and 2003 mainshocks focal mechanisms by Dolan and Bowman, 2004. Mesh-pattern shows the 1946 rupture area (Dolan et al., 1998). Inset: Tectonic diagram for the North Hispaniola-Puerto Rico margin. The red arrows indicate most representative GPS-derived velocities vectors showing the Hispaniola motion related to the North American plate (Calais et al., 2016). Bold black lines denote plate boundaries and major faults. HT: Hispaniola Trench; PRT: Puerto Rico Trench; BF: Bunce Fault; SOFZ: Septentrional-Oriente Fault Zone; EPGFZ: Enriquillo-Plaintain-Garden Fault Zone.

Fig. 2. Digital Elevation Model (DEM) derived from the multibeam bathymetry data and completed with data from GEBCO and SRTM dataset. Purple lines show the multi-channel seismic data from the FM0503 cruise (1980), and green lines show the single-channel seismic data from the MW8908 cruise (1989). Thicker lines mark the seismic sections shown in this paper labeled with the corresponding figure number. Red line marks the boundary of low resolution 150 m-gridded multibeam data from a compilation of USGS/NOAA cruises (Andrews et al., 2014). Dotted-black line shows the bathymetric profile path of the Figure 13.

Fig. 3 DEM as in Figure 2 showing the division into three morphostructural provinces: Bahamas Carbonate Province (BCP), Hispaniola Trench (HT) and Insular Margin (IM). The dashed brown line marks the island shelf edge. The red line marks the deformation front. The dashed black lines mark the base of the southern slope of BCP. The dashed blue lines mark the Bahamas

Banks shelf edge. Dashed lined boxes show the two regions used to describe the respective tectonic domains in the study area (Fig. 4: Oblique Underthrusting Domain; Fig. 5: Oblique Collision Domain)

Fig. 4 Morphostructural interpretation of the Oblique Underthrusting Domain. See location in Fig. 3.

Fig. 5 Morphostructural interpretation of the Oblique Collision Domain. See location in Fig. 3. See Fig. 4 for legend.

Fig. 6 A) Post-stack migrated MCS profile. See location in Fig. 2. V.E. is 3x on the seafloor. B) Line drawing interpretation.

Fig. 7 A) Stacked SCS profile. See location in Fig. 2. V.E. is 3x on the seafloor. B) Line drawing interpretation. See Figure 6B for legend.

Fig. 8 A) Post-stack migrated MCS profile. See location in Fig. 2. V.E. is 5x on the seafloor. B) Line drawing interpretation. See Figure 6B for legend.

Fig. 9 A) Stacked SCS profile. See location in Fig. 2. V.E. is 3x on the seafloor. B) Line drawing interpretation. See Figure 6B for legend.

Fig. 10 A) Stacked SCS profile. See location in Fig. 2. V.E. is 3x on the seafloor. B) Line drawing interpretation. See Figure 6B for legend.

Fig. 11 A) Stacked SCS profile. See location in Fig. 2. V.E. is 3x on the seafloor. B) Line drawing interpretation. See Figure 6B for legend.

Fig. 12 A) Stacked SCS profile. See location in Fig. 2. V.E. is 3x on the seafloor. B) Line drawing interpretation. See Figure 6B for legend.

Fig. 13 Bathymetric profile along the axial region of the Hispaniola Trench. Covers W to E the Hispaniola, Silver and Navidad basins. PRT: Puerto Rico Trench; OSD: Oblique Subduction Domain. See profile path in Figure 2 and Appendix A.

Fig. 14 A) Post-stack migrated MCS profile. See location in Fig. 2. V.E. is 3x on the seafloor. B) Line drawing interpretation. See Figure 6B for legend

Fig. 15 A) Stacked SCS profile. See location in Fig. 2. V.E. is 3x on the seafloor. B) Line drawing interpretation. See Figure 6B for legend.

Fig. 16 A) Stacked SCS profile. See location in Fig. 2. V.E. is 3x on the seafloor. B) Line drawing interpretation. See Figure 6B for legend.

Fig. 17 DEM as in Figure 5 showing focal mechanisms corresponding to the 1946 mainshock (in red is shown the focal mechanism by Russo and Villaseñor, 1995; in blue is shown the focal mechanism by Dolan et al., 1998). Mesh-pattern shows the 1946 rupture area. Red lines show the coastal areas affected by the tsunami.

App. A. Contour map of the study region. Black lines are 200 m contours. Major contour interval each 1,000 m. Blue line shows the profile path from Figure 13.

App. B. Bathymetric 3D image of the study area seen from the western end of the Puerto Rico Trench. The three morphostructural provinces (Bahamas Carbonate Province, Hispaniola Trench and Insular Margin) and the two tectonic domains present in the study area (Oblique Collision and Oblique Underthrusting domains) are shown. The vertical exaggeration is 5x.

App. C. Gradient map (degrees) of the three regions in the study area. See legend for color interpretation.

Highlights:

Northern Hispaniola Margin is studied with new high-resolution bathymetry and vintage seismic data.

Northern Hispaniola Deformed Belt forms an active N-verging fold-and-thrust imbricate system.

Gravity failures are frequent features in the Northern Hispaniola Margin and Bahamas Banks slope.

Oblique collision accelerates the Bahamas Carbonate Province collapse and retreat.

New observations help the assessment of tsunami hazards in the Northern Caribbean region.

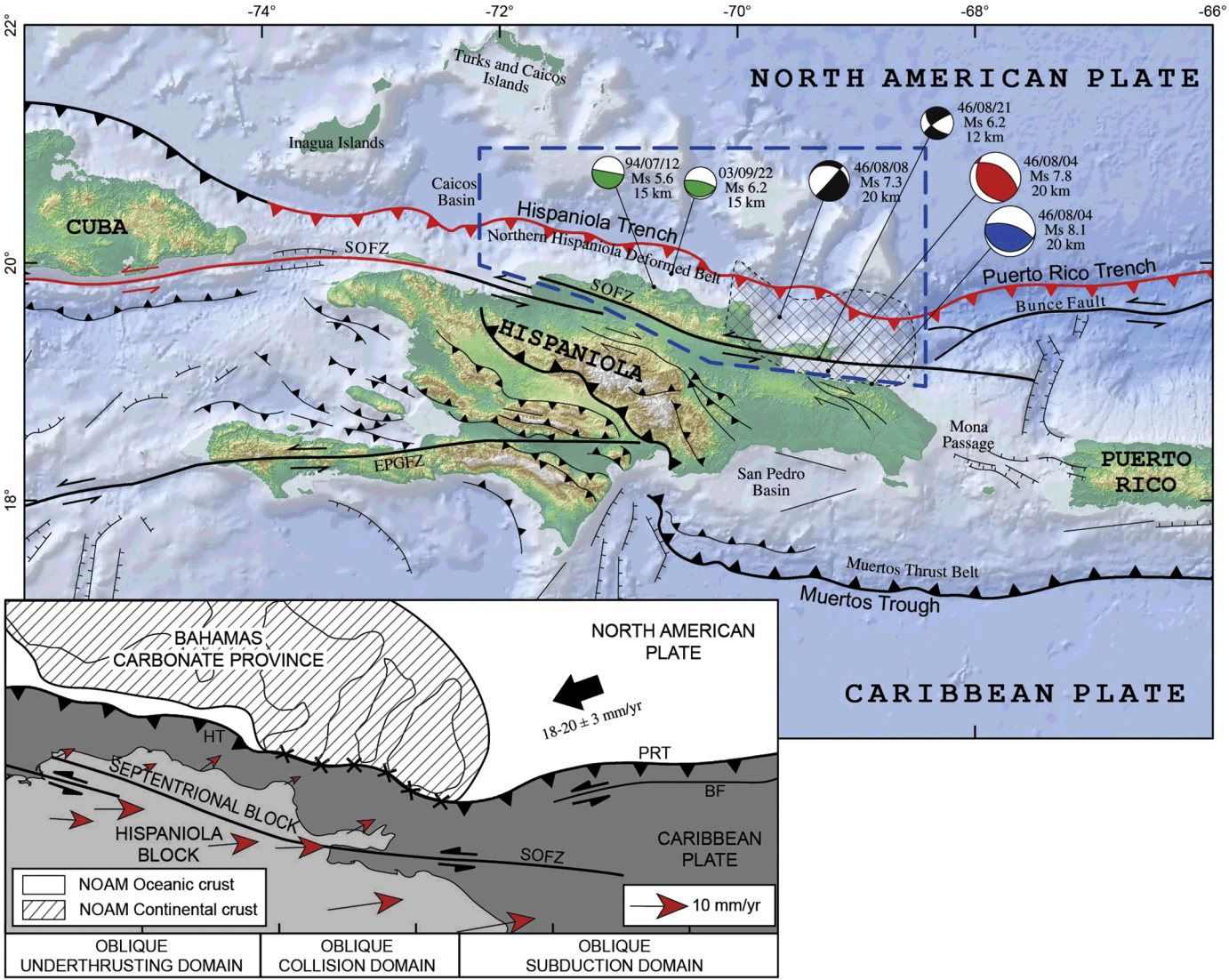
-74°
-72°
-70°
-68°
-66°
22°
20°
18°
NORTH AMERICAN PLATE
Turks and Caicos Islands
Inagua Islands
Caicos Basin
CUBA
SOFZ
Hispaniola Trench
Northern Hispaniola Deformed Belt
94/07/12 Ms 5.6 15 km
03/09/22 Ms 6.2 15 km
46/08/08 Ms 7.3 20 km
46/08/21 Ms 6.2 12 km
46/08/04 Ms 7.8 20 km
46/08/04 Ms 8.1 20 km
Puerto Rico Trench
Bunce Fault
HISPANIOLA
EPGFZ
Mona Passage
PUERTO RICO
San Pedro Basin
Muertos Thrust Belt
Muertos Trough
CARIBBEAN PLATE
BAHAMAS CARBONATE PROVINCE
NORTH AMERICAN PLATE
18-20 ± 3 mm/yr
HT
PRT
BF
SEPTENTRIONAL BLOCK
HISPANIOLA BLOCK
CARIBBEAN PLATE
SOFZ
NOAM Oceanic crust
NOAM Continental crust
10 mm/yr
OBLIQUE UNDERTHRUSTING DOMAIN
OBLIQUE COLLISION DOMAIN
OBLIQUE SUBDUCTION DOMAIN

Figure 1

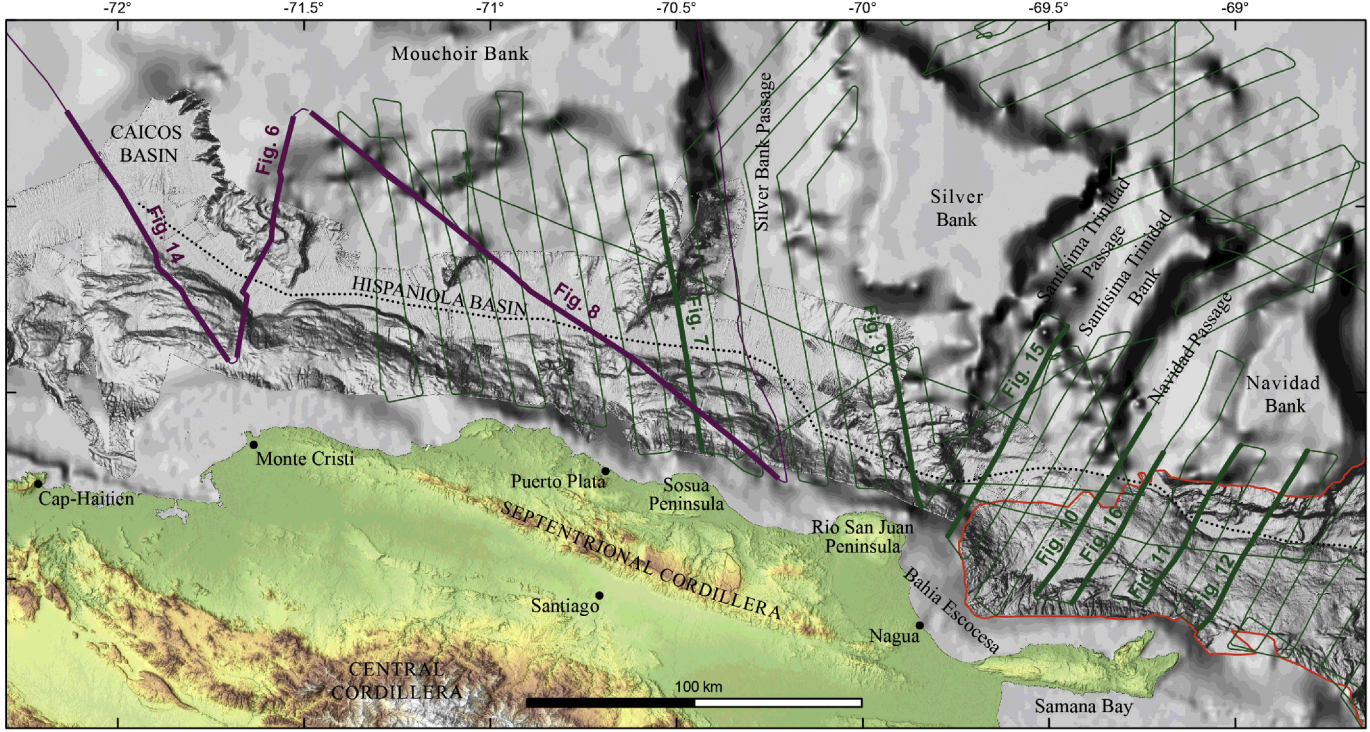
-72°
-71.5°
-71°
-70.5°
-70°
-69.5°
-69°
21°
20.5°
20°
19.5°
Mouchoir Bank
CAICOS BASIN
Fig. 6
Fig. 14
HISPANIOLA BASIN
Fig. 8
Fig. 7
Fig. 9
Silver Bank Passage
Silver Bank
Santisima Trinidad Passage
Santisima Trinidad Bank
Fig. 15
Navidad Passage
Navidad Bank
Monte Cristi
Cap-Haitien
Puerto Plata
Sosua Peninsula
SEPTENTRIONAL CORDILLERA
Rio San Juan Peninsula
Fig. 10
Fig. 16
Fig. 11
Fig. 12
Bahia Escocesa
Santiago
Nagua
CENTRAL CORDILLERA
100 km
Samana Bay

Figure 2

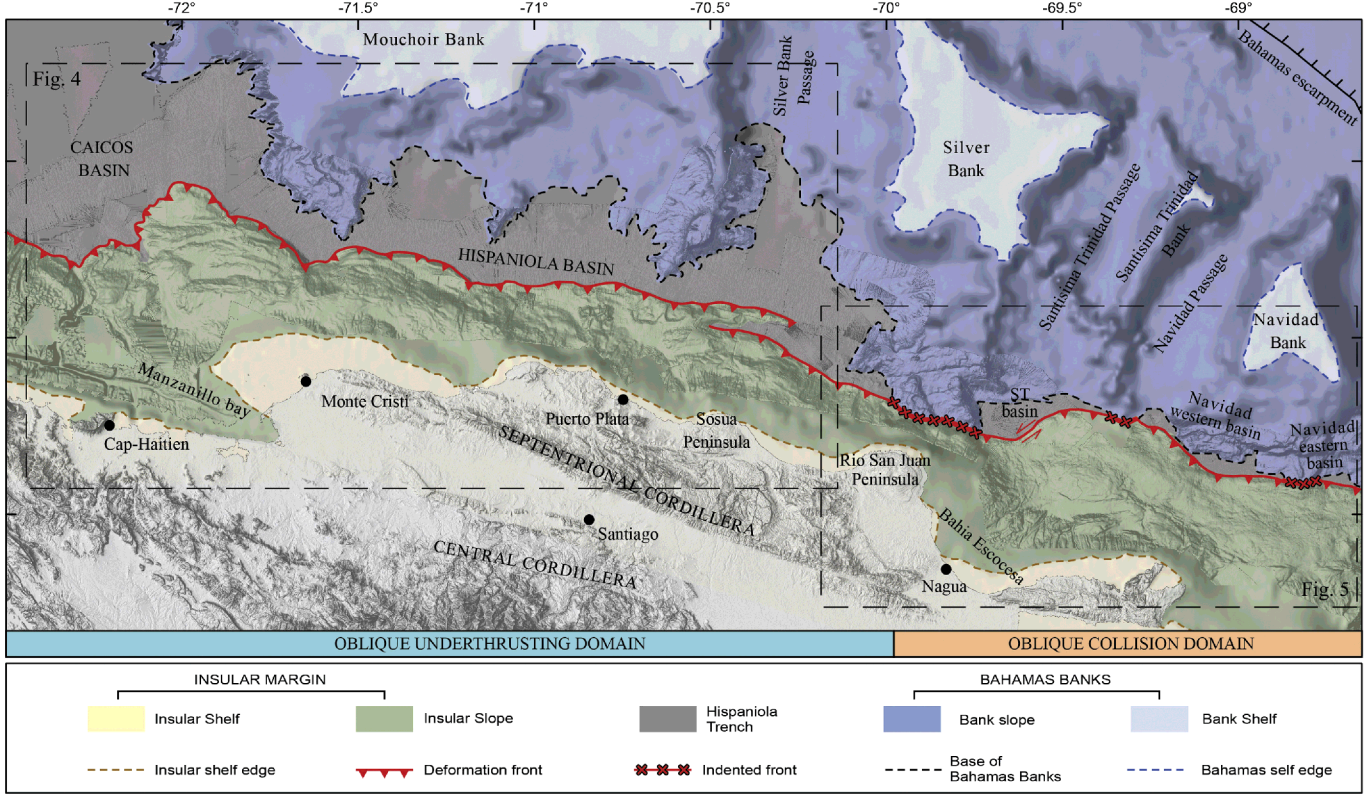
-72°
-71.5°
-71°
-70.5°
-70°
-69.5°
-69°
20.5°
20°
19.5°
Mouchoir Bank
Fig. 4
CAICOS BASIN
Silver Bank Passage
Bahamas escarpment
Silver Bank
HISPANIOLA BASIN
Santisima Trinidad Passage
Santisima Trinidad Bank
Navidad Passage
Navidad Bank
Manzanillo bay
Monte Cristi
Puerto Plata
Sosua Peninsula
ST basin
Navidad western basin
Navidad eastern basin
Cap-Haitien
SEPTENTRIONAL CORDILLERA
Rio San Juan Peninsula
Bahia Escocesa
Santiago
CENTRAL CORDILLERA
Nagua
Fig. 5
OBLIQUE UNDERTHRUSTING DOMAIN
OBLIQUE COLLISION DOMAIN
INSULAR MARGIN
Insular Shelf
Insular Slope
Hispaniola Trench
BAHAMAS BANKS
Bank slope
Bank Shelf
Insular shelf edge
Deformation front
Indented front
Base of Bahamas Banks
Bahamas self edge

Figure 3

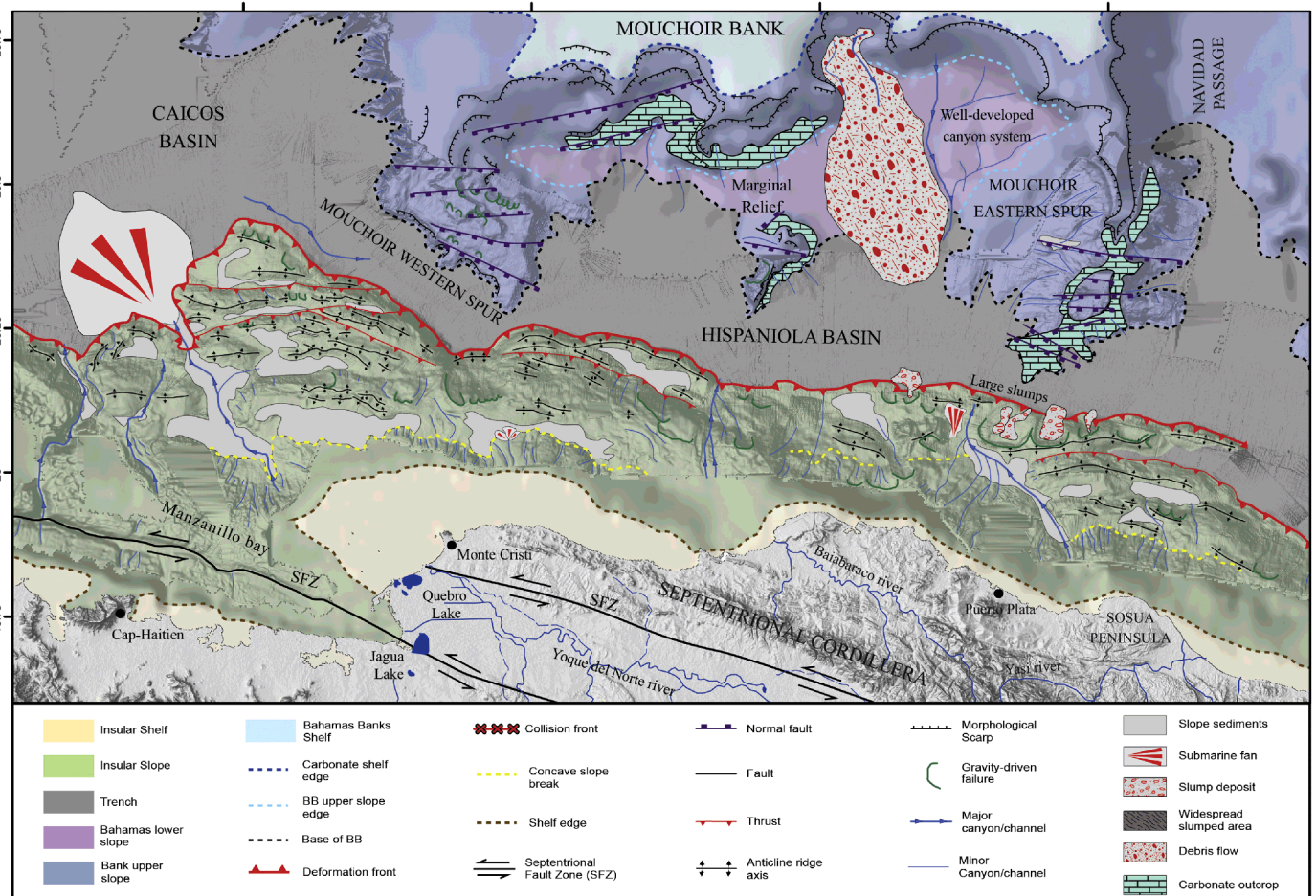
-72°
-71.5°
-71°
-70.5°
20.75°
20.5°
20.25°
20°
19.75°
MOUCHOIR BANK
CAICOS BASIN
NAVIDAD PASSAGE
Well-developed canyon system
Marginal Relief
MOUCHOIR EASTERN SPUR
MOUCHOIR WESTERN SPUR
HISPANIOLA BASIN
Large slumps
Manzanillo bay
SFZ
Monte Cristi
Quebro Lake
SFZ
SEPTENTRIONAL CORDILLERA
Baiabaraco river
Puerto Plata
SOSUA PENINSULA
Cap-Haitien
Jagua Lake
Yoque del Norte river
Yasi river
Insular Shelf
Insular Slope
Trench
Bahamas lower slope
Bank upper slope
Bahamas Banks Shelf
Carbonate shelf edge
BB upper slope edge
Base of BB
Deformation front
Collision front
Concave slope break
Shelf edge
Septentrional Fault Zone (SFZ)
Normal fault
Fault
Thrust
Anticline ridge axis
Morphological Scarp
Gravity-driven failure
Major canyon/channel
Minor Canyon/channel
Slope sediments
Submarine fan
Slump deposit
Widespread slumped area
Debris flow
Carbonate outcrop

Figure 4

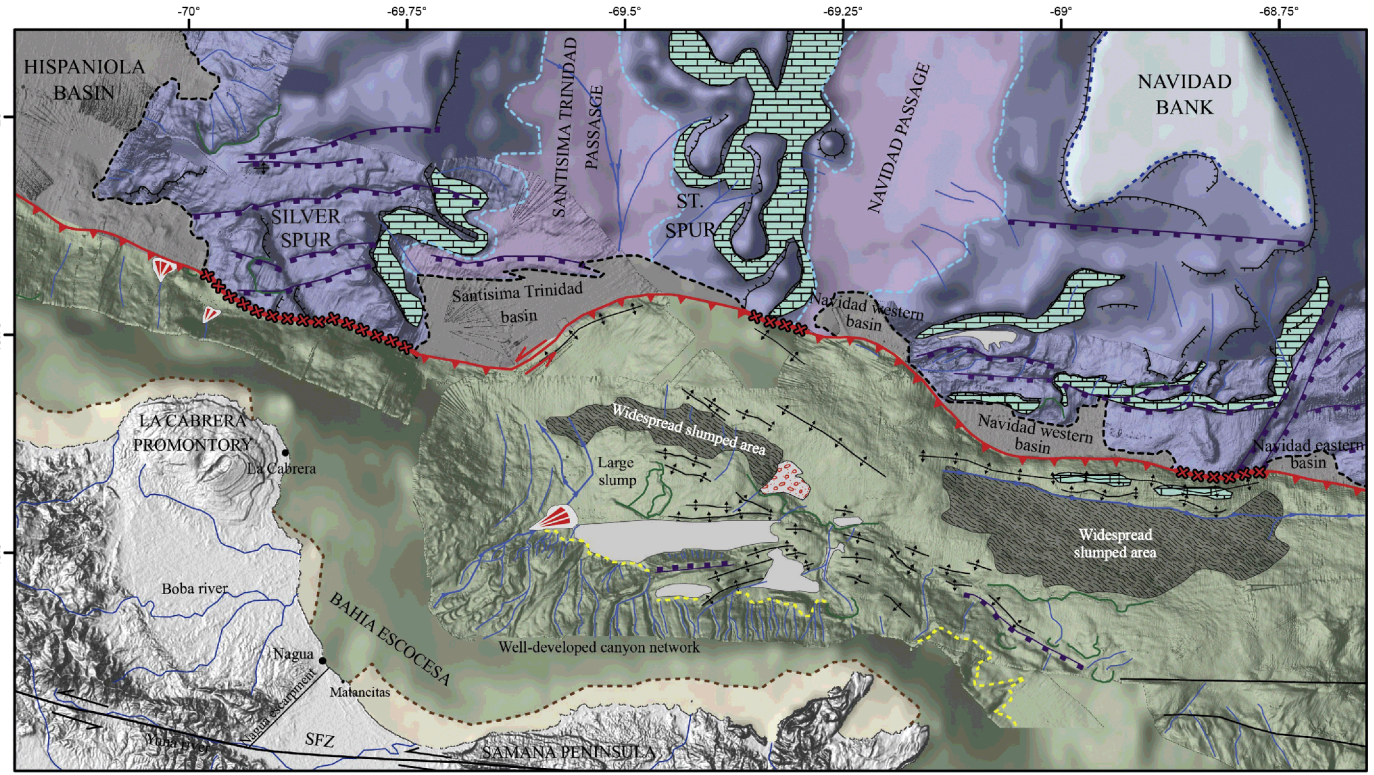
-70°
-69.75°
-69.5°
-69.25°
-69°
-68.75°
20°
19.75°
19.5°
HISPANIOLA BASIN
SILVER SPUR
SANTISIMA TRINIDAD PASSAGE
ST. SPUR
NAVIDAD PASSAGE
NAVIDAD BANK
Santisima Trinidad basin
Navidad western basin
Navidad western basin
Navidad eastern basin
Widespread slumped area
Large slump
Widespread slumped area
LA CABRERA PROMONTORY
La Cabrera
Boba river
BAHIA ESCOCESA
Well-developed canyon network
Nagua
Matancitas
Escarpment
SFZ
SAMANA PENINSULA

Figure 5

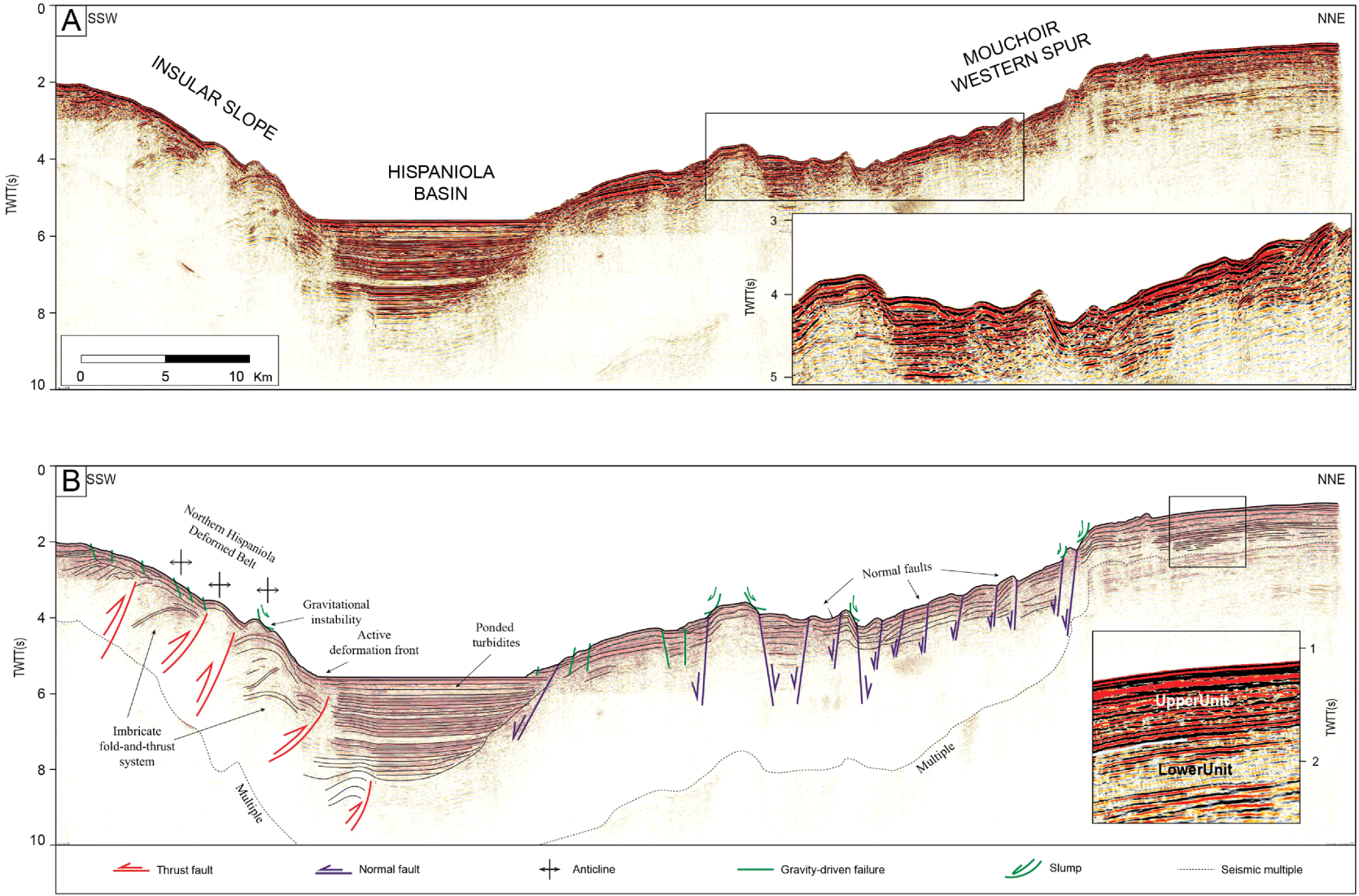
A
SSW
NNE
INSULAR SLOPE
HISPANIOLA BASIN
MOUCHOIR WESTERN SPUR
TWTT(s)
0
5
10 Km
B
Northern Hispaniola Deformed Belt
Gravitational instability
Active deformation front
Ponded turbidites
Normal faults
Imbricate fold-and-thrust system
Multiple
UpperUnit
LowerUnit
Thrust fault
Normal fault
Anticline
Gravity-driven failure
Slump
Seismic multiple

Figure 6

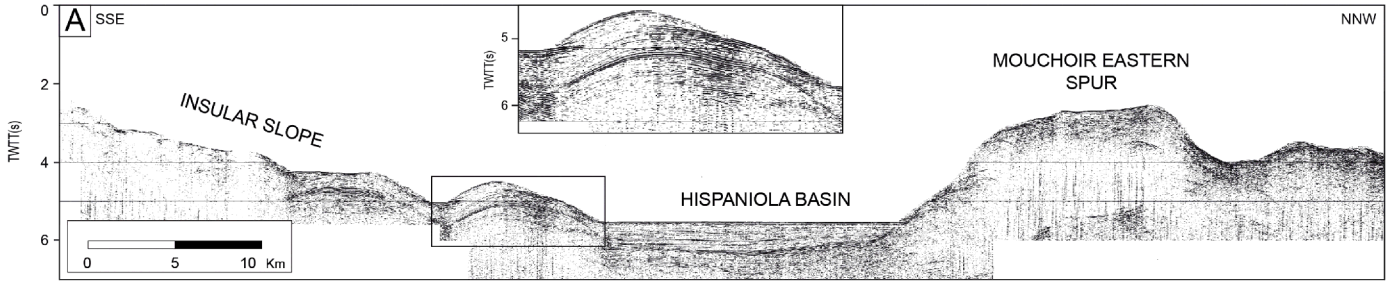
A
SSE
NNW
TWTT(s)
0
2
4
6
INSULAR SLOPE
HISPANIOLA BASIN
MOUCHOIR EASTERN SPUR
5
6
0
5
10 Km

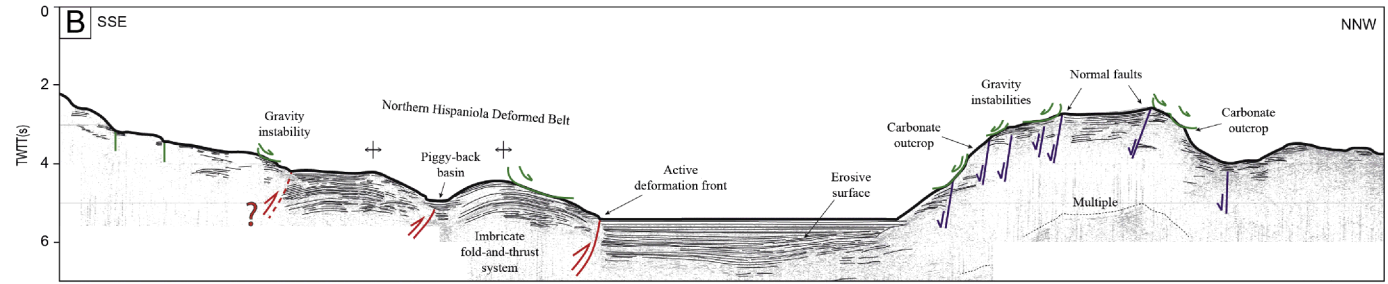
B
SSE
NNW
TWTT(s)
0
2
4
6
Gravity instability
Northern Hispaniola Deformed Belt
Piggy-back basin
Active deformation front
Erosive surface
Imbricate fold-and-thrust system
Gravity instabilities
Normal faults
Carbonate outcrop
Carbonate outcrop
Multiple
?

Figure 7

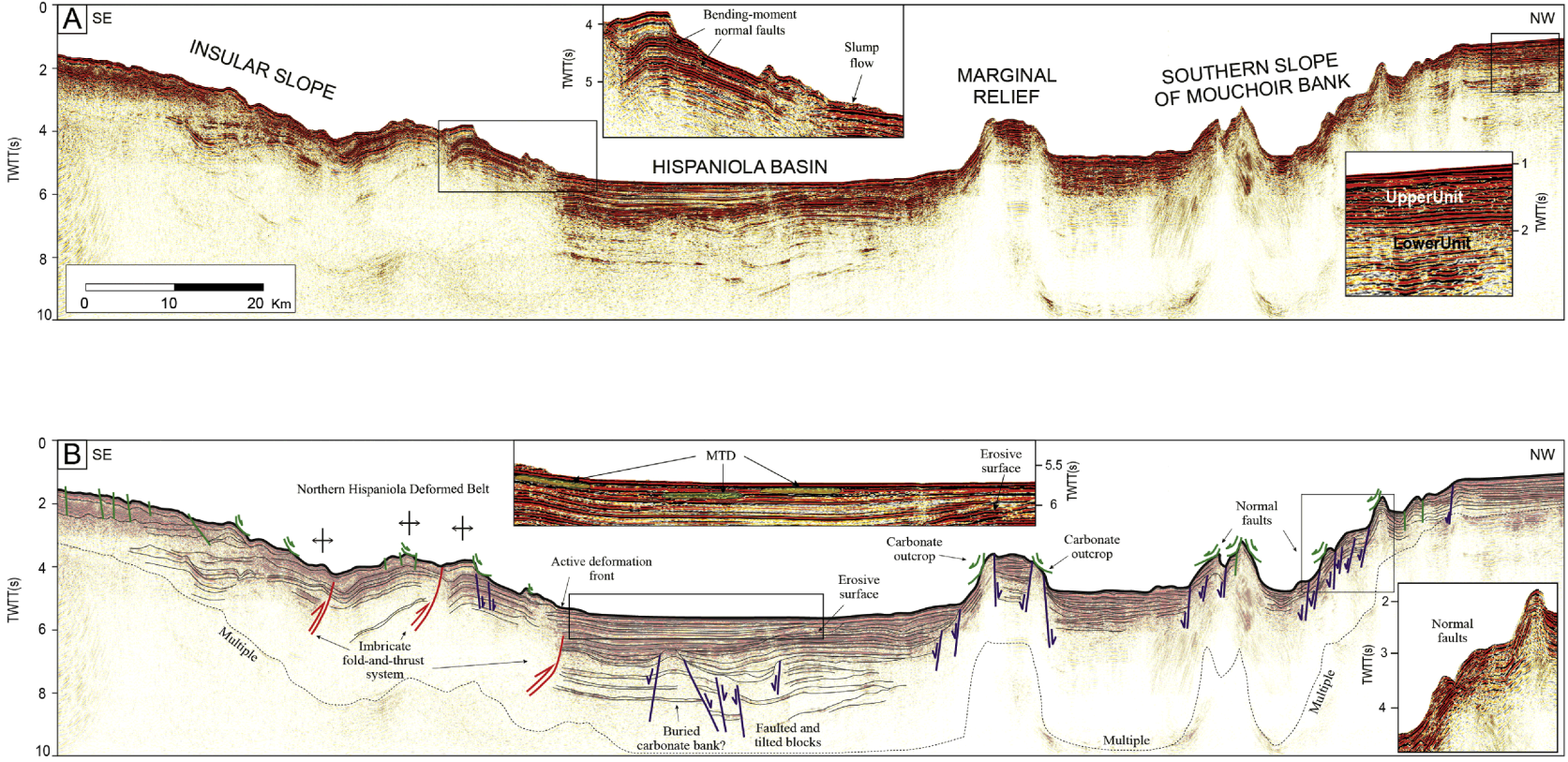
A
SE
NW
INSULAR SLOPE
HISPANIOLA BASIN
MARGINAL RELIEF
SOUTHERN SLOPE OF MOUCHOIR BANK
Bending-moment normal faults
Slump flow
UpperUnit
LowerUnit
TWTT(s)
0
10
20 Km
B
SE
NW
Northern Hispaniola Deformed Belt
MTD
Erosive surface
Active deformation front
Carbonate outcrop
Carbonate outcrop
Normal faults
Normal faults
Imbricate fold-and-thrust system
Multiple
Buried carbonate bank?
Faulted and tilted blocks
Multiple
Multiple
TWTT(s)

Figure 8

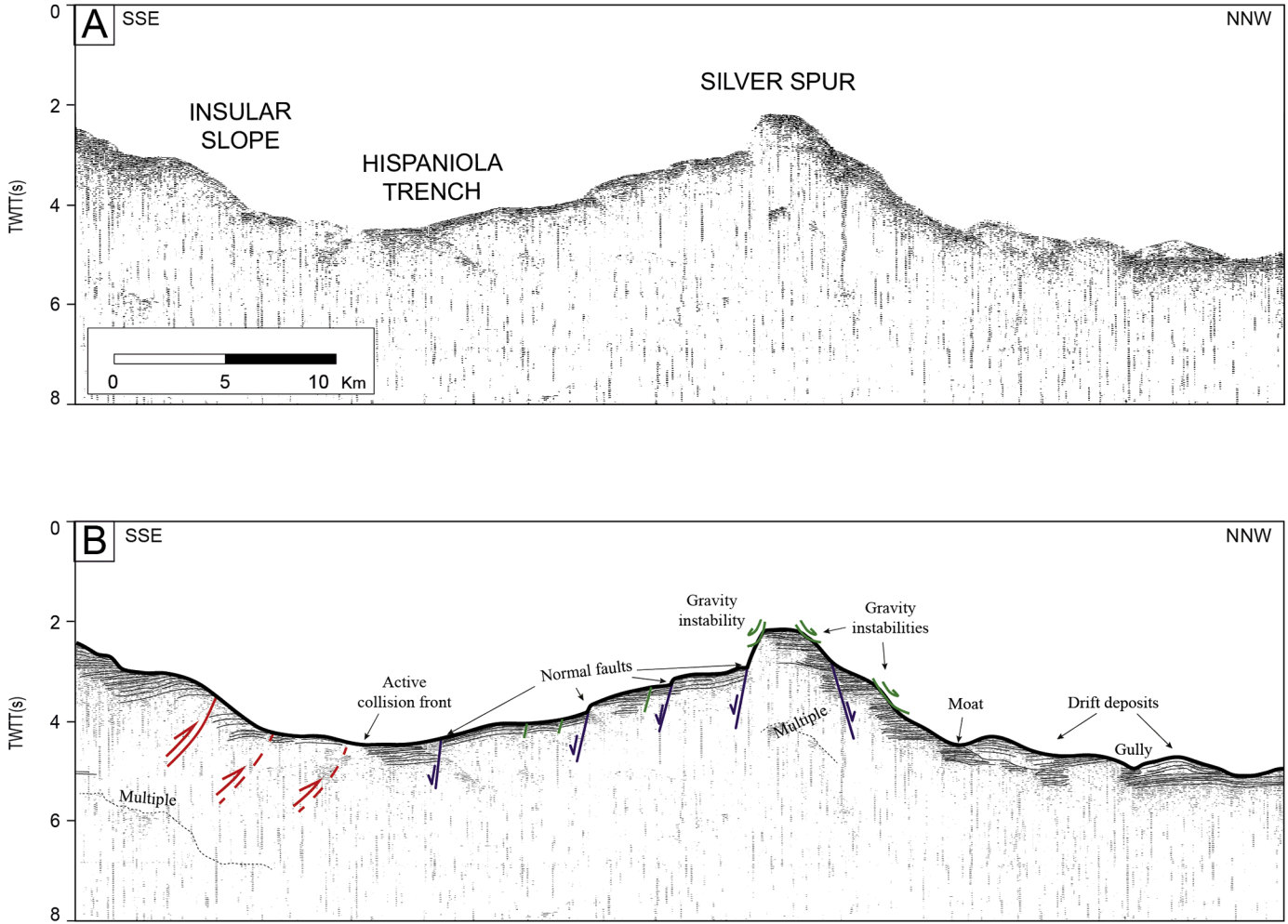
A
SSE
NNW
INSULAR SLOPE
HISPANIOLA TRENCH
SILVER SPUR
TWTT(s)
0
2
4
6
8
0
5
10 Km
B
SSE
NNW
Gravity instability
Gravity instabilities
Active collision front
Normal faults
Multiple
Moat
Drift deposits
Gully
Multiple

Figure 9

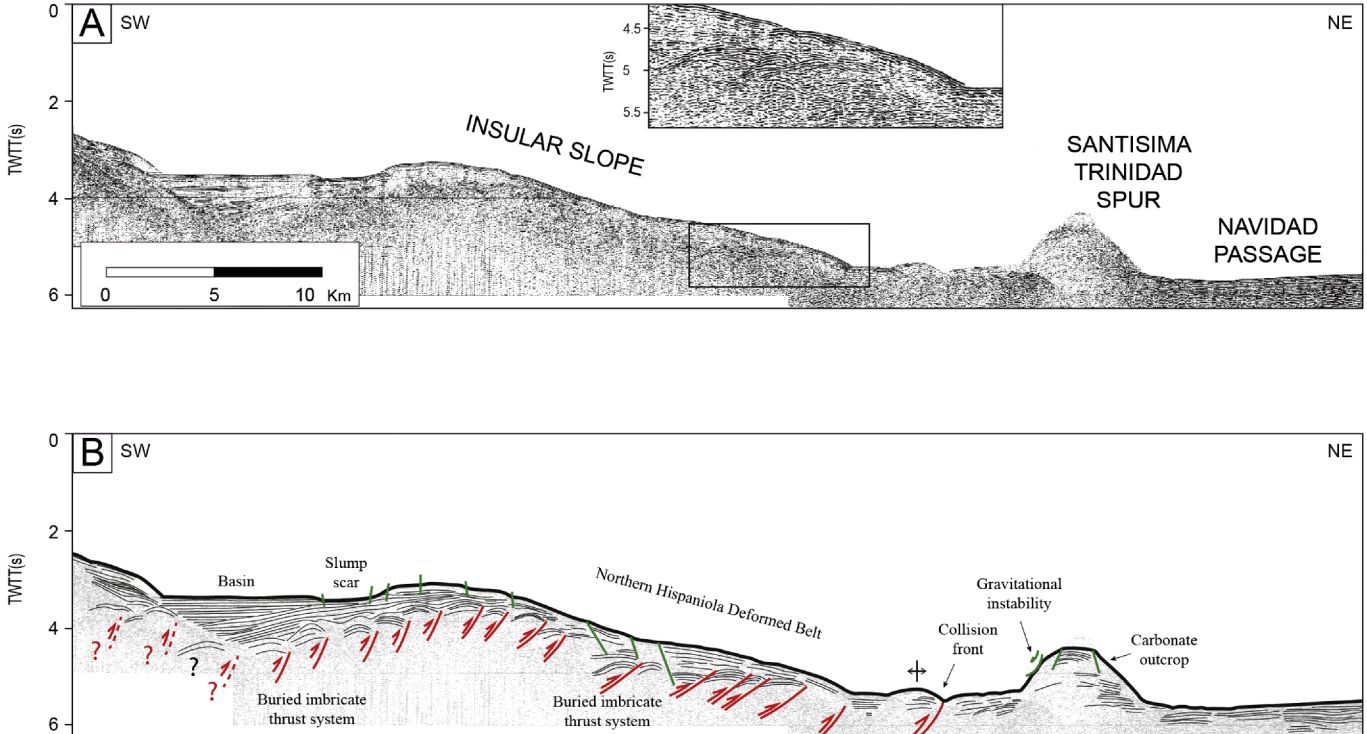
A
SW
NE
TWTT(s)
0
2
4
6
4.5
5
5.5
INSULAR SLOPE
SANTISIMA
TRINIDAD
SPUR
NAVIDAD
PASSAGE
0
5
10 Km
B
SW
NE
Basin
Slump
scar
Northern Hispaniola Deformed Belt
Gravitational
instability
Collision
front
Carbonate
outcrop
Buried imbricate
thrust system
Buried imbricate
thrust system

Figure 10

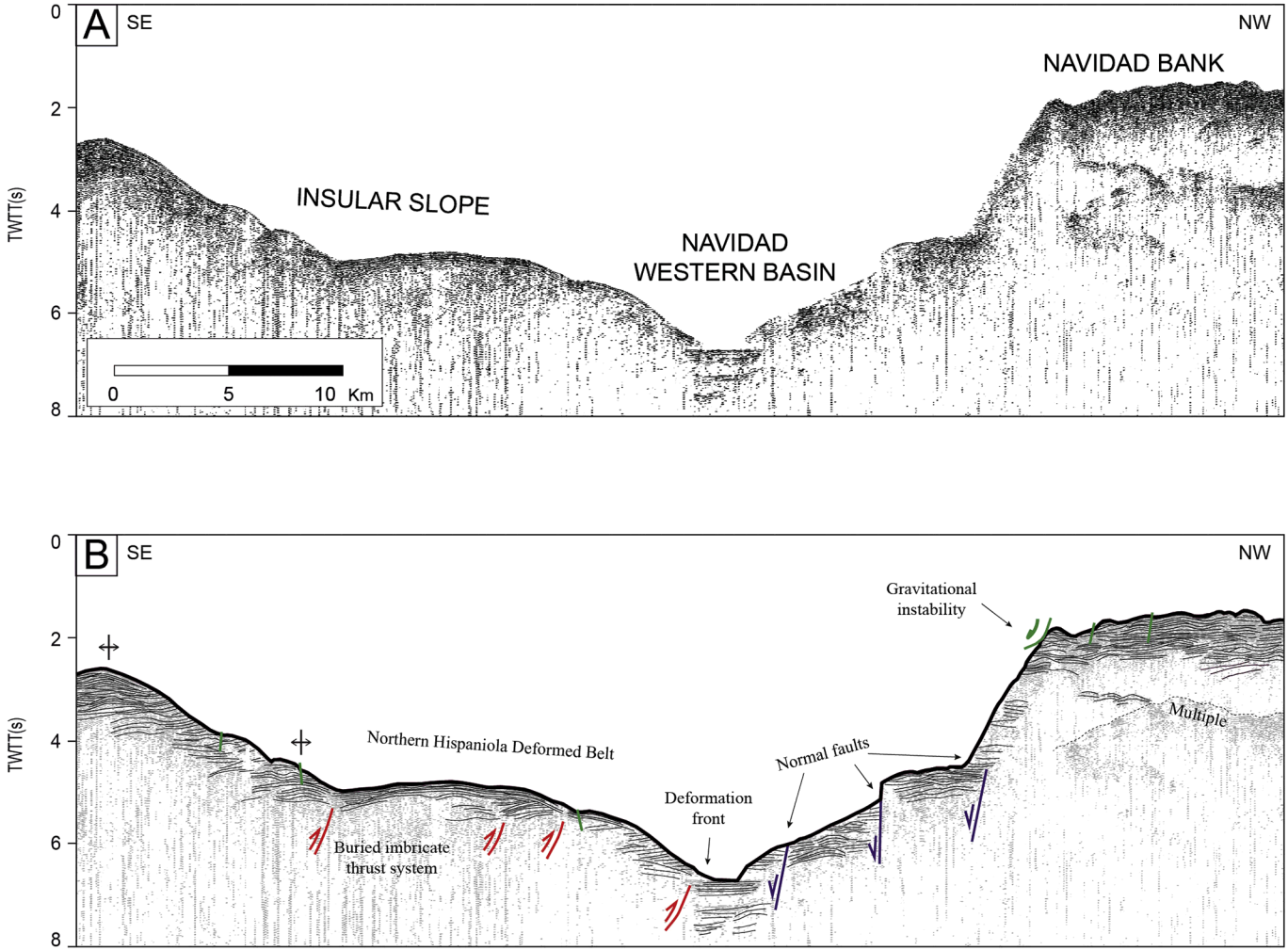
A
SE
NW
NAVIDAD BANK
INSULAR SLOPE
NAVIDAD
WESTERN BASIN
0
5
10 Km
TWTT(s)
0
2
4
6
8
B
SE
NW
Gravitational
instability
Multiple
Northern Hispaniola Deformed Belt
Normal faults
Deformation
front
Buried imbricate
thrust system
TWTT(s)
0
2
4
6
8

Figure 11

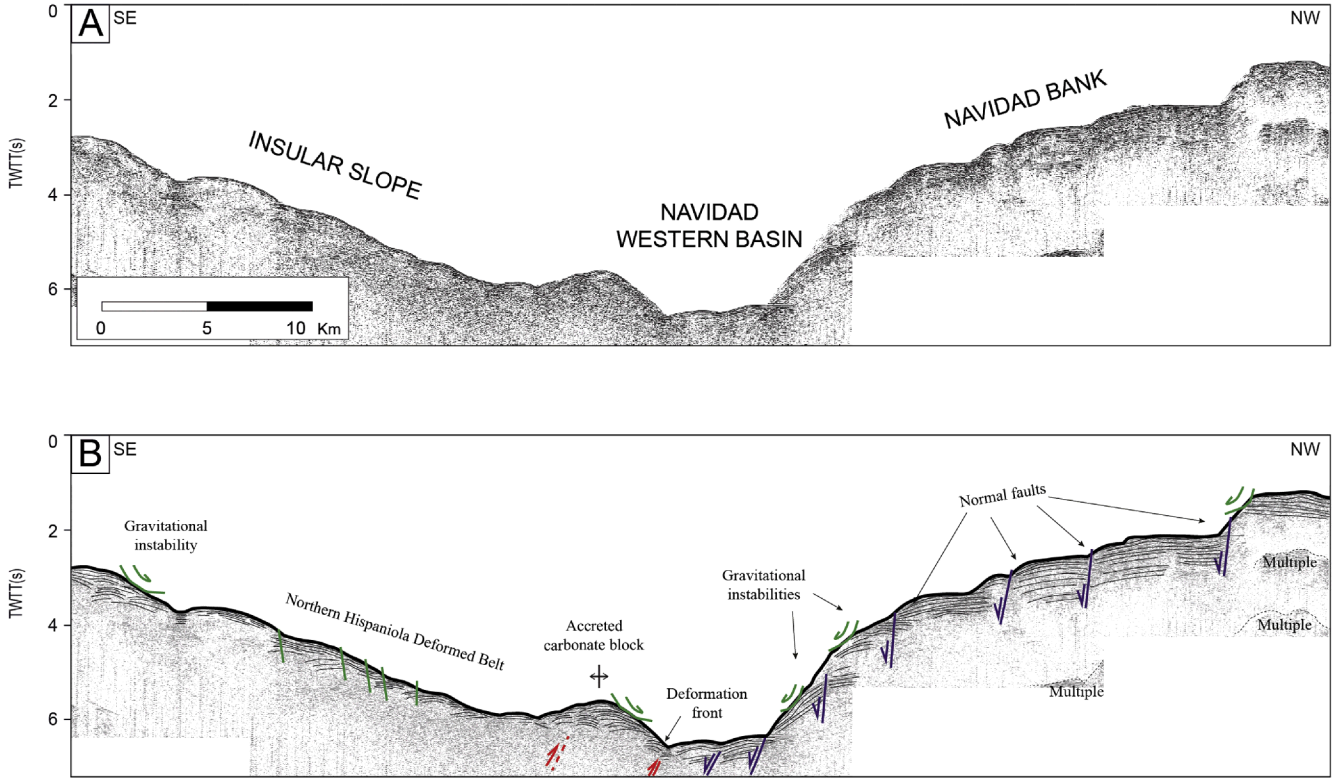
A
SE
NW
TWTT(s)
0
2
4
6
INSULAR SLOPE
NAVIDAD BANK
NAVIDAD
WESTERN BASIN
0
5
10 Km
B
SE
NW
TWTT(s)
Gravitational
instability
Northern Hispaniola Deformed Belt
Accreted
carbonate block
Deformation
front
Gravitational
instabilities
Normal faults
Multiple
Multiple
Multiple

Figure 12

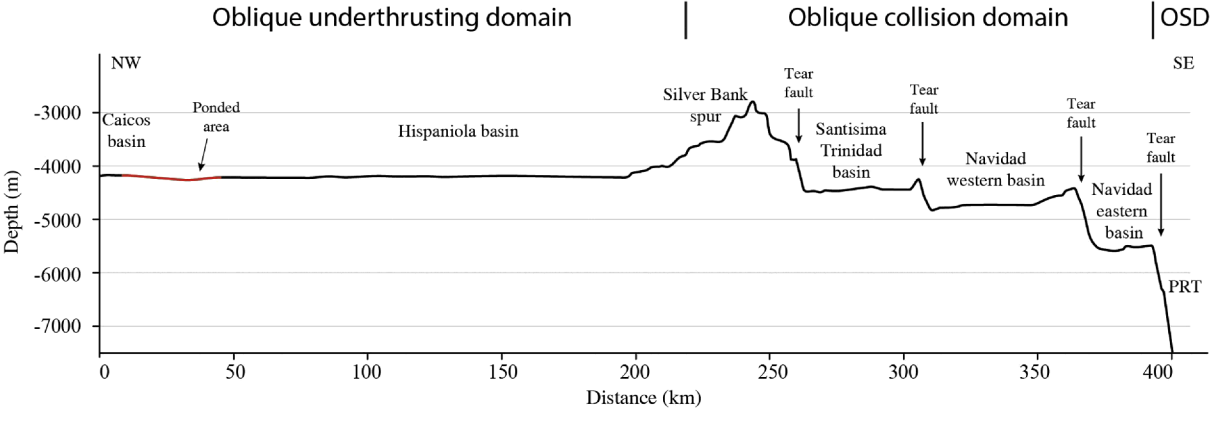
Oblique underthrusting domain
Oblique collision domain
OSD
NW
SE
Caicos basin
Ponded area
Hispaniola basin
Silver Bank spur
Tear fault
Santisima Trinidad basin
Tear fault
Navidad western basin
Tear fault
Navidad eastern basin
Tear fault
PRT
Depth (m)
-3000
-4000
-5000
-6000
-7000
0
50
100
150
200
250
300
350
400
Distance (km)

Figure 13

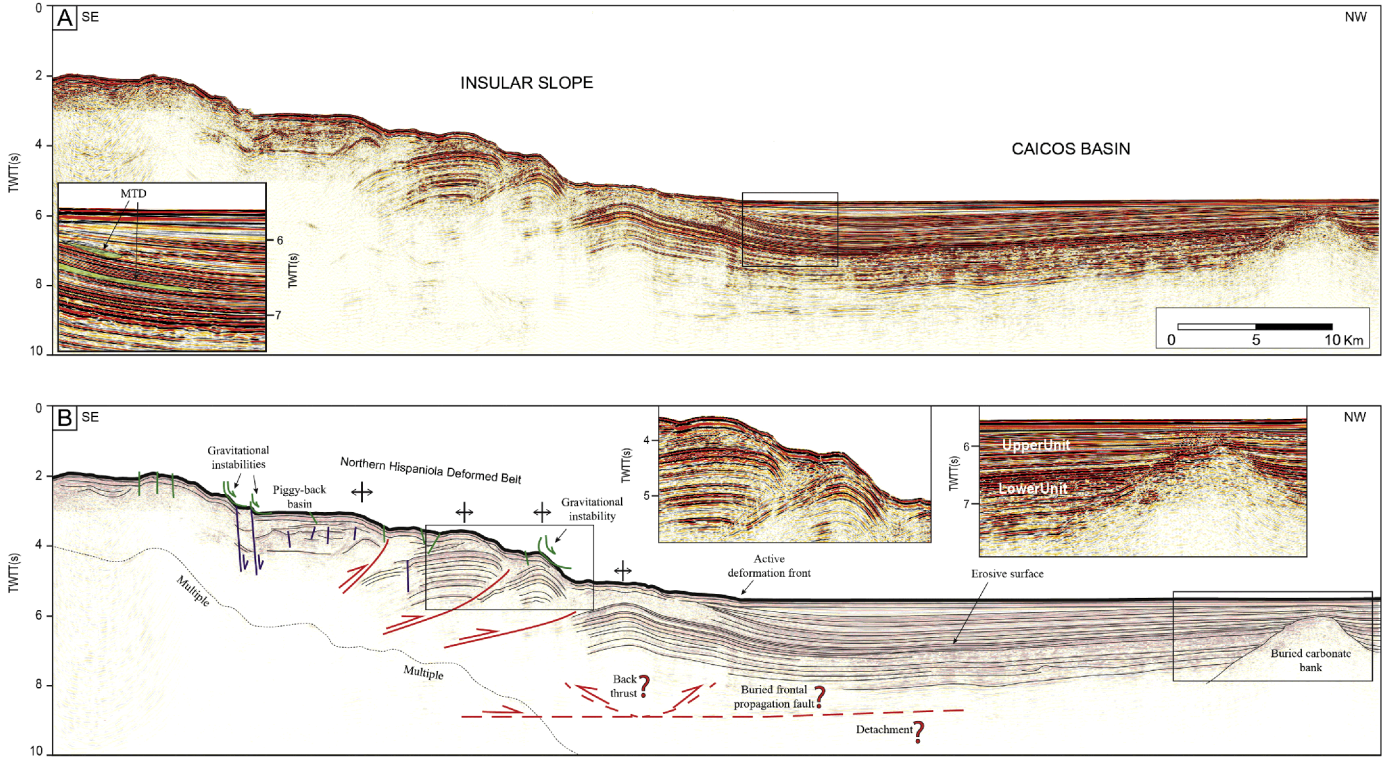
A
SE
NW
INSULAR SLOPE
CAICOS BASIN
MTD
TWTT(s)
0
2
4
6
8
10
0
5
10 Km
B
SE
NW
Gravitational instabilities
Piggy-back basin
Northern Hispaniola Deformed Belt
Gravitational instability
Active deformation front
Erosive surface
UpperUnit
LowerUnit
Multiple
Multiple
Back thrust
Buried frontal propagation fault
Detachment
Buried carbonate bank

Figure 14

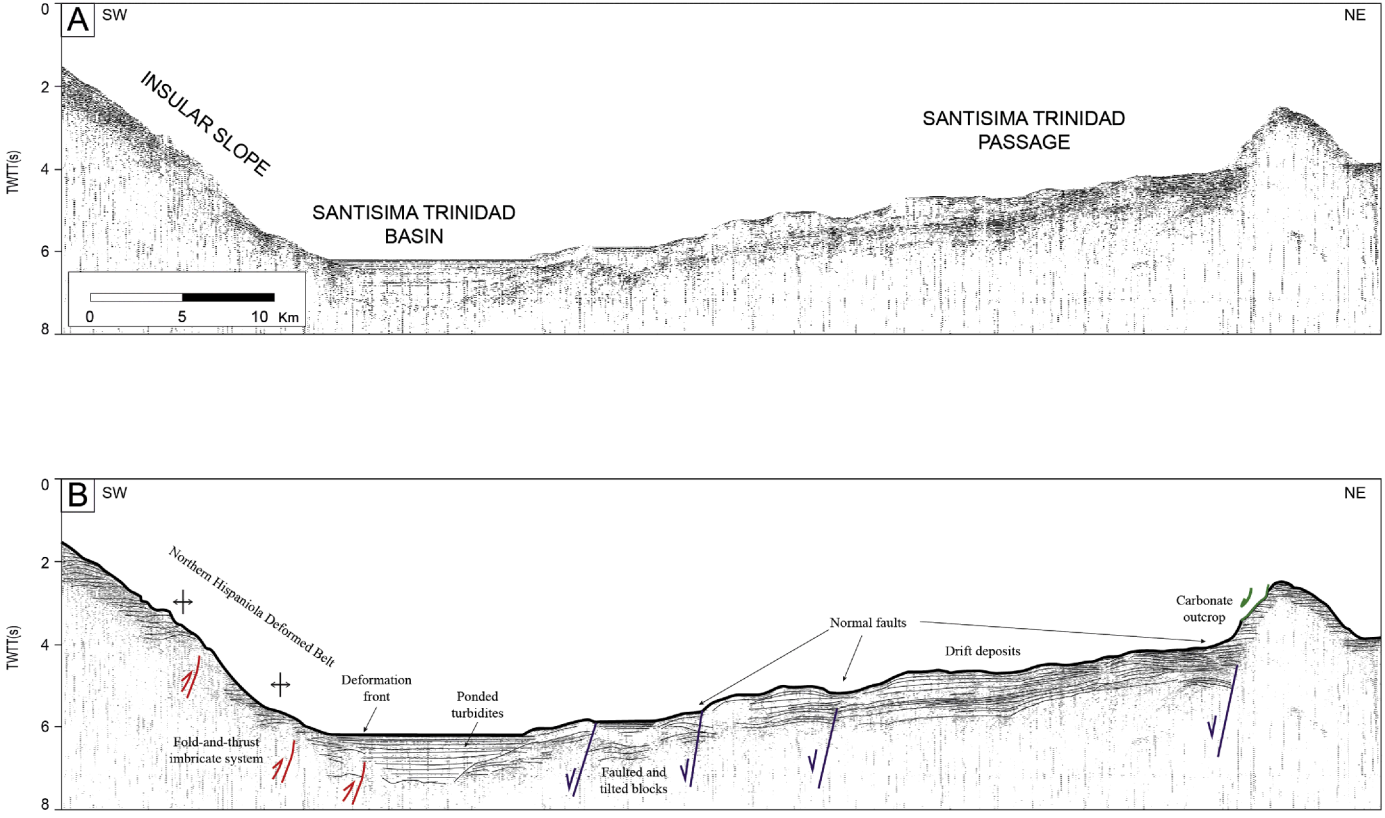
A
SW
NE
INSULAR SLOPE
SANTISIMA TRINIDAD
BASIN
SANTISIMA TRINIDAD
PASSAGE
0
5
10 Km
TWTT(s)
0
2
4
6
8
B
SW
NE
Northern Hispaniola Deformed Belt
Deformation
front
Ponded
turbidites
Fold-and-thrust
imbricate system
Faulted and
tilted blocks
Normal faults
Drift deposits
Carbonate
outcrop
TWTT(s)
0
2
4
6
8

Figure 15

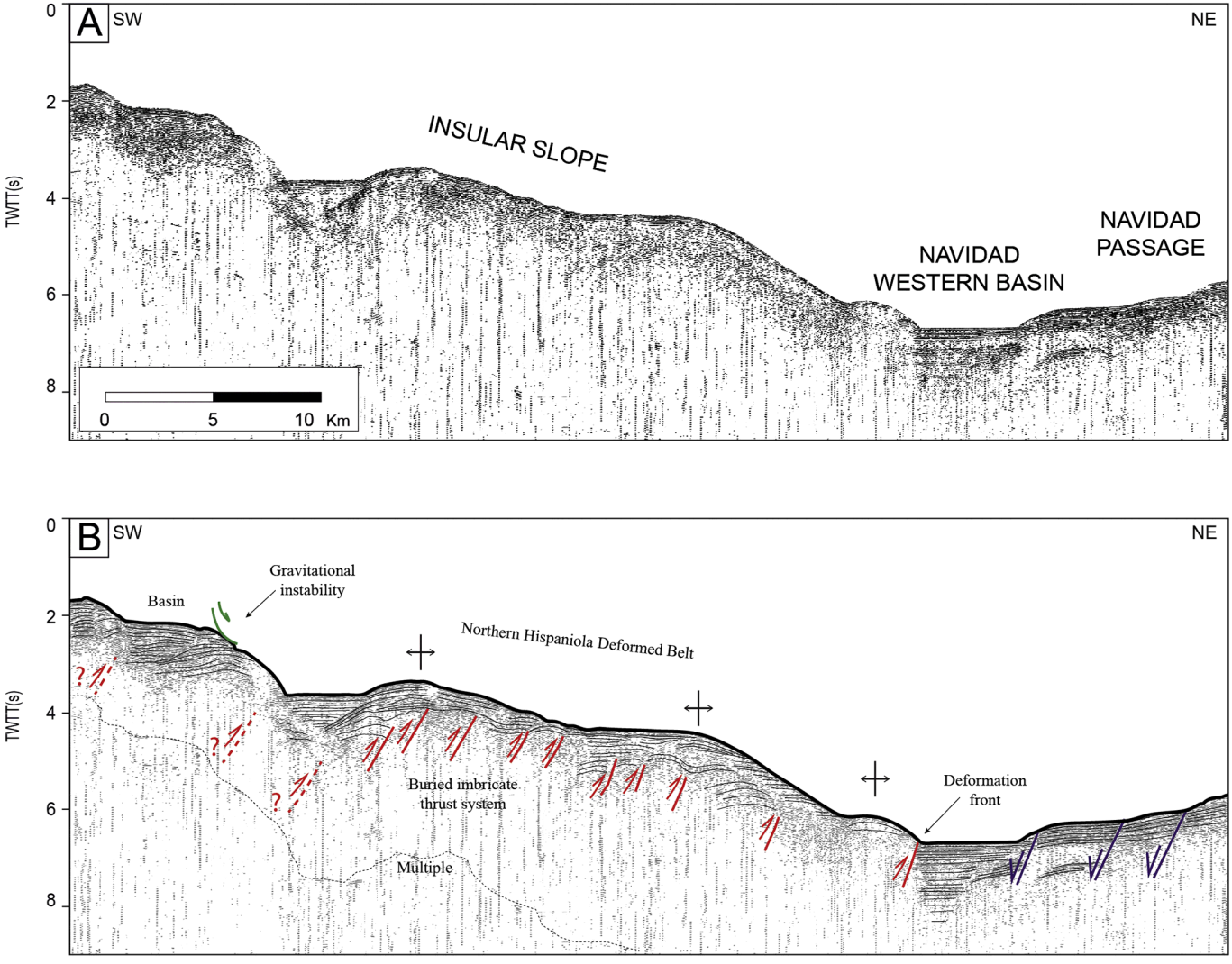
A
SW
NE
INSULAR SLOPE
NAVIDAD
WESTERN BASIN
NAVIDAD
PASSAGE
TWTT(s)
0
2
4
6
8
0
5
10 Km
B
SW
NE
Basin
Gravitational
instability
Northern Hispaniola Deformed Belt
Buried imbricate
thrust system
Multiple
Deformation
front
TWTT(s)
0
2
4
6
8

Figure 16

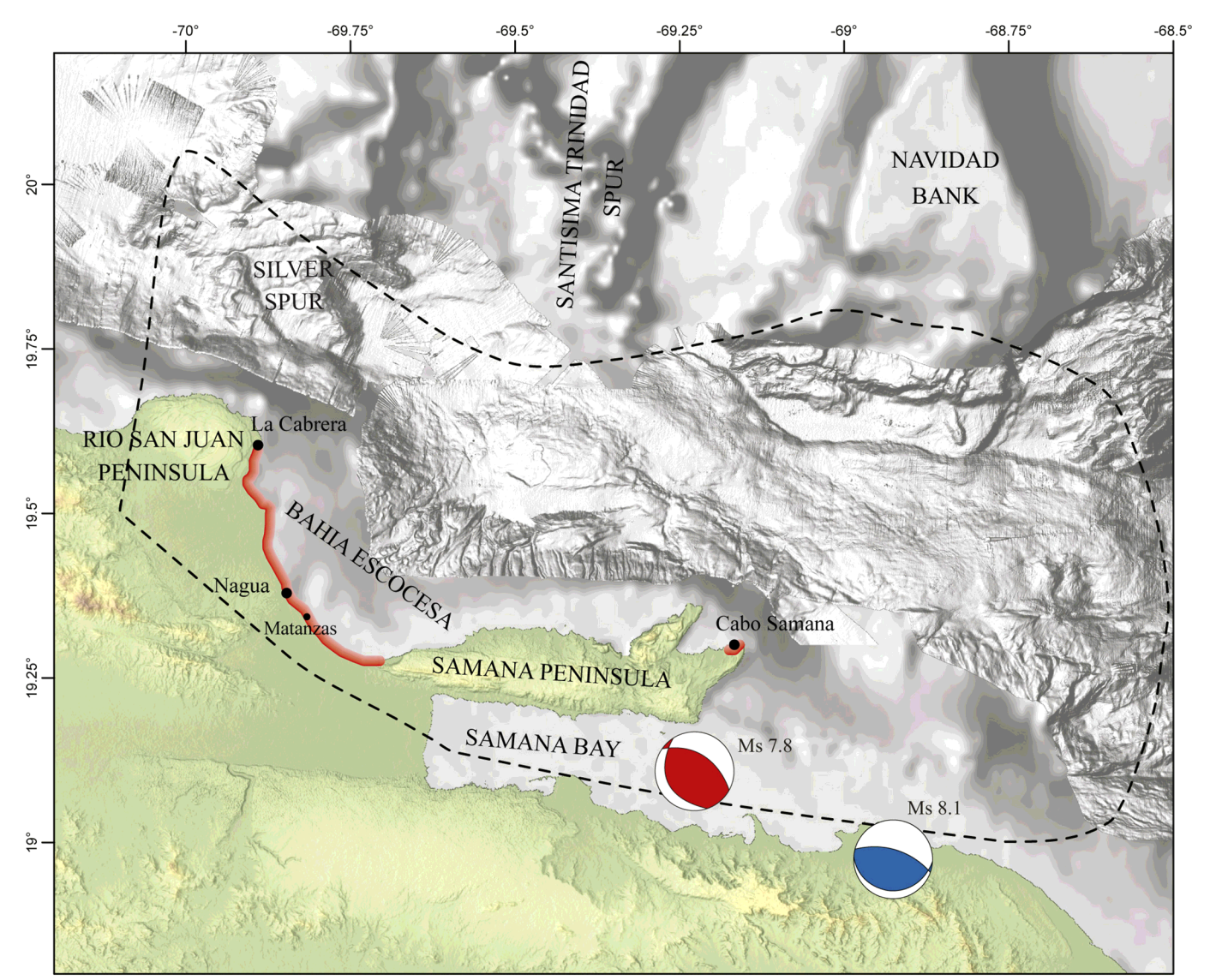
-70°
-69.75°
-69.5°
-69.25°
-69°
-68.75°
-68.5°
20°
19.75°
19.5°
19.25°
19°
SILVER SPUR
SANTISIMA TRINIDAD SPUR
NAVIDAD BANK
RIO SAN JUAN PENINSULA
La Cabrera
BAHIA ESCOCESA
Nagua
Matanzas
Cabo Samana
SAMANA PENINSULA
SAMANA BAY
Ms 7.8
Ms 8.1

Figure 17